

TKK Dissertations 26
Espoo 2006

NUMERICAL MODELING IN ELECTRO- AND MAGNETOENCEPHALOGRAPHY

Doctoral Dissertation

I. Oğuz Tanzer



**Helsinki University of Technology
Department of Engineering Physics and Mathematics
Laboratory of Biomedical Engineering**

TKK Dissertations 26
Espoo 2006

NUMERICAL MODELING IN ELECTRO- AND MAGNETOENCEPHALOGRAPHY

Doctoral Dissertation

I. Oğuz Tanzer

Dissertation for the degree of Doctor of Science in Technology to be presented with due permission of the Department of Engineering Physics and Mathematics for public examination and debate in Auditorium F1 at Helsinki University of Technology (Espoo, Finland) on the 13th of March, 2006, at 12 noon.

**Helsinki University of Technology
Department of Engineering Physics and Mathematics
Laboratory of Biomedical Engineering**

**Teknillinen korkeakoulu
Teknillisen fysiikan ja matematiikan osasto
Lääketieteellisen tekniikan laboratorio**

Distribution:

Helsinki University of Technology
Department of Engineering Physics and Mathematics
Laboratory of Biomedical Engineering
P.O. Box 2200
FI - 02015 TKK
FINLAND
Tel. +358-9-451 3172
Fax +358-9-451 3182
URL: <http://biomed.tkk.fi/>
E-mail: oguz.tanzer@tkk.fi

© 2006 I. Oğuz Tanzer

ISBN 951-22-8090-6
ISBN 951-22-8091-4 (PDF)
ISSN 1795-2239
ISSN 1795-4584 (PDF)
URL: <http://lib.tkk.fi/Diss/2006/isbn9512280914/>

TKK-DISS-2108

Otamedia Oy
Espoo 2006



HELSINKI UNIVERSITY OF TECHNOLOGY P.O. BOX 1000, FI-02015 TKK http://www.tkk.fi	ABSTRACT OF DOCTORAL DISSERTATION
Author	
Name of the dissertation	
Date of manuscript	Date of the dissertation
Monograph	Article dissertation (summary + original articles)
Department	
Laboratory	
Field of research	
Opponent(s)	
Supervisor (Instructor)	
Abstract	
Keywords	
ISBN (printed)	ISSN (printed)
ISBN (pdf)	ISSN (pdf)
ISBN (others)	Number of pages
Publisher	
Print distribution	
The dissertation can be read at http://lib.tkk.fi/Diss/	

Academic dissertation

Laboratory of Biomedical Engineering
Department of Engineering Physics and Mathematics
Helsinki University of Technology

Numerical modeling in electro- and magnetoencephalography

Author: I. Oğuz Tanzer
Department of Engineering Physics and Mathematics
Laboratory of Biomedical Engineering
Helsinki University of Technology

Supervising professor: Doc. Risto Ilmoniemi

Instructors: Doc. Jukka Nenonen,
Laboratory of Biomedical Engineering,
Department of Engineering Physics and Mathematics,
Helsinki University of Technology.

Prof. Erkki Somersalo,
Department of Mathematics,
Helsinki University of Technology.

Preliminary examiners: Prof. Jens Haueisen, University of Jena, Germany.
Prof. Pasi Karjalainen, University of Kuopio, Finland.

Official opponent: Matti Hämäläinen,
Associate Professor of Radiology,
Harvard Medical School
Boston, Massachusetts, USA.

Publications

This Thesis consists of the present summary and the following publications:

- P1 Gençer N. G., **Tanzer I. O.**, Özdemir K., Acar C. and Sungur M. (1998). State of art in realistic head modeling for electromagnetic source imaging of the human brain, *Elektrik*, 6:167–182.
- P2 Gençer N. G. and **Tanzer I. O.** (1999). Forward problem solution of electromagnetic source imaging using a new BEM formulation with high order elements, *Phys. Med. Biol.*, 44:2275–2287.
- P3 Gençer N. G., Acar C. E. and **Tanzer I. O.** (2003). Forward problem solution of magnetic source imaging, *Magnetic Source Imaging of the Human Brain*, Eds: Zhong-Lin Lu, Lloyd Kaufman, Lawrence Erlbaum Associates Inc, ISBN 0805845119: 77–100.
- P4 **Tanzer I. O.**, Järvenpää S., Nenonen J. and Somersalo E. (2003). Effect of potential approximation on linear inversion from surface potential and magnetic field, *Biomed. Tech.*, 48:254–257.
- P5 **Tanzer I. O.**, Järvenpää S., Nenonen J. and Somersalo E. (2005). Representation of bioelectric current sources using Whitney elements in the finite element method, *Phys. Med. Biol.*, 50:3023–3039.
- P6 **Tanzer I. O.**, Järvenpää S. and Somersalo E. (2005). An alternative formulation to represent bioelectric current sources using Whitney elements, *Helsinki University of Technology Report TKK-F-A840*.

Contributions of the author

The primary contribution by the author of this Thesis is the numerical evaluation of the forward problem solution of electromagnetic source imaging in the brain with the boundary element and finite element method. The included publications are the result of shared work with the co-authors. In publication P1, together with the principal author and other coauthors we designed and performed computational experiments. The computational part concerning BEM was performed by me. I have written parts of the general theory of P1 and all of the section on boundary element modeling. In P2, the principal author proposed the research idea and I contributed in establishing the research plan. I designed and implemented the computer simulations, proposed the error comparison method and equally contributed to writing the whole paper. For P3, the principal author proposed the numerical comparison of BEM and FEM as a research idea. The principal author was responsible for writing the manuscript, but I actively participated in writing the section on boundary element modeling and parts of the general theory section. I have also edited the document in general. In publications P4–P6, I was the principal author and I actively contributed to the design and development of the theoretical concept. The implementation of the finite element method in publications P4–P6 was done in collaboration with the second author. I designed and carried out the simulations, testing and interpretation of results with the proposed methods. I wrote most of the parts of publications P4–P6, but the other authors also participated in editing the manuscript.

Table of contents

List of publications	iii
Table of contents	v
Abbreviations	vii
List of symbols	viii
Preface	ix
1 Introduction	1
2 EEG and MEG in brain research	3
2.1 Origin of signals	3
2.2 Electrochemical reactions in neurons	4
2.3 The cerebral cortex	5
2.4 Measuring bioelectromagnetic fields	7
2.4.1 EEG, the measure of bioelectric field	7
2.4.2 MEG, the measure of biomagnetic field	8
3 Theory and modeling of bioelectromagnetic fields	11
3.1 Maxwell's equations	11
3.1.1 Quasi-static approximation	12
3.2 Current dipole as a source model	13
3.3 Volume conductor models	14
3.3.1 \mathbf{B} and V for infinite volume conductor	15
3.3.2 \mathbf{B} and V for piecewise homogeneous conductor	15
3.4 Modeling the head	17
3.4.1 Single sphere model	17
3.4.2 Multiple spheres model	18
3.4.3 Realistic Head Models	18
3.4.4 Closed form solutions for \mathbf{B} and V	21
4 Numerical solution of the forward problem	23
4.1 BEM with isoparametric elements, (P2)	23
4.1.1 Triangular isoparametric surface elements	24
4.1.2 Implementation of the isoparametric BEM formulation	24
4.2 Galerkin BEM with singularity extraction (P4)	27
4.3 FEM with Whitney Elements (P5)	28
4.3.1 Calculation of the electric potential	30
4.3.2 Calculation of the magnetic field	31

5	Numerical simulations	33
5.1	Error measure	33
5.2	BEM simulations of EEG with isoparametric elements (P1–P3)	33
5.2.1	Homogeneous sphere model	34
5.2.2	Concentric shell model	35
5.3	BEM simulations of EEG/MEG with singularity extraction technique (P4)	35
5.4	FEM simulations of EEG and MEG with Whitney elements (P5,P6) .	36
5.4.1	Continuous source coefficients	37
6	Discussion	41
6.1	BEM studies, (P1– P4)	41
6.1.1	Factors affecting the performance of BEM, (P2)	42
6.2	FEM studies	43
6.2.1	FEM studies with Whitney elements, (P5, P6)	43
6.3	Comparison of BEM and FEM, (P1, P3)	44
6.4	Effects of tissue conductivity anisotropy	45
6.5	Future developments	46
7	Conclusions	47
	Bibliography	49

Abbreviations

BEM	Boundary element method
CSF	Cerebrospinal fluid
CT	Computed tomography
ECD	Equivalent current dipole
ECG	Electrocardiography
EEG	Electroencephalogram, electroencephalography
EIT	Electrical impedance tomography
EMSI	Electromagnetic source imaging
FEM	Finite element method
GMRES	Generalized minimal residual method
IPA	Isolated potential approach
MAG	Magnification factor
MAP	Maximum a posteriori
MCG	Magnetocardiography
MEG	Magnetoencephalography
MRI	Magnetic resonance image
PET	Positron emission tomography
PSP	Postsynaptic potential
RDM	Relative difference measure
RMS	Root mean square
SPECT	Single photon emission tomography
SQUID	Superconducting quantum interference device

List of symbols

r, \mathbf{r}_f	Observation, field location
r', \mathbf{r}_0	Source location
\mathbf{n}	Unit normal
\mathbf{J}	Conduction current density (ampere/m ²)
\mathbf{J}_p	Primary current density
\mathbf{J}_s	Secondary (volume) current density
\mathbf{E}	Electric field (volt/m)
V	Electric potential (volt)
V_0	Electric potential in infinite space (volt)
\mathbf{D}	Electric displacement (coulomb/m ²)
\mathbf{B}	Magnetic flux density (tesla)
\mathbf{H}	Magnetic field (ampere/m)
$\sigma(x), \sigma$	Conductivity of the medium (siemens/m)
ϵ	Permittivity of the medium (farad/m)
ρ	Charge density (coulomb/m ³)
\mathbf{q}	Current dipole
$u(x), u$	Potential distribution
u^h	FEM approximation of u
Ω	Volume conductor
$\partial\Omega$	Boundary of Ω
δ	Dirac delta function
P_n	Legendre polynomial of n^{th} order
P_n^m	Associated Legendre polynomial of n^{th} order, m^{th} degree

Preface

The basis of this Thesis work started in Middle East Technical University and was continued in BioMag Laboratory, Helsinki and Laboratory of Biomedical Engineering, Helsinki University of Technology. The publications P5 and P6 and the summary of the Thesis were completed at the Brain Research Unit of the Low Temperature Laboratory.

Completing this doctoral work has been a wonderful and often overwhelming experience. It is hard to know whether the challenge has been the subject itself or how to write a paper, give a coherent talk, work in a group, recover a crashed hard drive, stay up until the birds start singing or to arduous fight with myself resisting to procrastination while there is a lot of work to do.

I have been very privileged to have undoubtedly work with very intuitive, smart and supportive people during this work. Prof. Nevzat Gençer of Electrical Engineering Department, Middle East Technical University, introduced me to brain research from a small chat and has been an extremely motivating advisor during my earlier work, without his initial guidance on my academic research, ethics and practicality this Thesis would never have happened.

I would like to thank Doc. Jukka Nenonen for being my advisor during my later studies giving essential guidance and help, without his full support this Thesis would not have been possible. Doc. Risto Ilmoniemi made it possible for me to come to Finland. He has supported me throughout my studies both as an advisor and as supervisor. Dr. Ilmoniemi's wonderful leadership while head of BioMag Laboratory certainly was an immense motivation both for the laboratory and for this Thesis to be realized. I would like to thank Prof. Toivo Katila, for his contributions to the biomedical engineering department and to HUT during his vice rectorship. He has provided attentive advice and support as my supervisor throughout my studies.

Many thanks to simply wonderful Prof. Erkki Somersalo, for all the support and motivation, inverse days and jokes. His mathematical work has been the basis of my study, without his full support this Thesis would not have been possible.

My most intense academic cooperation has been with Dr. Seppo Järvenpää, whose ability, mathematical knowledge, his promptness and eagerness to help at all times has been a role model for me. All the off-topic conversations we had while working were the great side benefits of our collaboration, again without his full support this Thesis would not have been possible.

I would like to thank Prof. Riitta Hari, director of the Brain Research Unit in Low Temperature Laboratory for the great motivation and support during the final part of the Thesis work. I would also like to thank Prof. Mikko Paalanen for successfully managing and maintaining an unparalleled wonderful and warm research environment in the Low Temperature Laboratory.

Throughout my 4 years, I was supported for many semesters by the MADAME project of the Finnish Academy. The Graduate School of Functional Studies in Medicine has provided support through the generosity of my advisors. I thank CIMO (Centre for International Mobility) for providing me the initial funding to start my studies in Finland. I would like to thank Biomedicum foundation and Tekniikan edistämissäätiö (TES)

for supporting my research.

Special thanks also go to the support personnel, from Laboratory of Biomedical Engineering, Ms. Leena Meilahti, Ms. Taru Bister and Ms. Satu Koskela and from Low Temperature Laboratory, Ms. Liisi Pasanen, Ms. Pirjo Kinanen, Ms. Satu Pakarinen and to Ms. Tuire Koivisto are surely the kindest, most helpful persons one could possibly hope to depend on administrative matters.

There are countless others who have been there for me throughout my time as a graduate student. Dr. M. Nejat Tek, Dr. M. Kemal Özdemir, Dr. Barış Kazar, Dr. Yeşim Serinağaoğlu, Dr. Leena Lauronen, Dr. Elina Pihko, Dr. Johanna Karen Pallesen, Mr. Christopher Bailey, Dr. Klaus Linkenkaer-Hansen, Mr. Juha Heiskala stand out as both good, caring friends and providers of fascinating conversations.

I am personally grateful to Prof. Yorgo I Stefanopoulos for his support and sharing his vast insight on everything. I have not seen similar ability to master, on one hand, the administrative and social issues, and on the other hand, realizing academic excellence. He has been a truly great leader in the development of Institute of Biomedical Engineering, Boğaziçi University and has also been a role model for many engineers coming out of this institution. His legacy will surely be remembered forever. I would also like to thank Prof. Yekta Ülgen, Prof. Mehmed Özkan, Doc. Albert Güveniş, Doc. Ahmet Ademoğlu and Doc. Halil Özcan Gülçür for interesting discussions and support for my studies in Boğaziçi University. I would also like to thank Ms. Berrin Kocayurt for being open, helpful and smiling at all times.

I was always interested in engineering and physics but my fascination with medical sciences is due to the influence of my mother Prof. Dr. Fatoş Neşe Tanzer and my father Dr. Tevfik Fikret Tanzer. They also kept me sane during the my hardest times via all communication channels available from Turkey.

Finally, my wife Arzu has been the most important person for me over the years in many aspects. In our stormy relationship she has seen my best and my worst.

Otaniemi, October 2005

Ihsan Oğuz Tanzer

Her zaman yanımda olan aileme adıyorum...

Chapter 1

Introduction

The human brain is an extremely complex and organized structure that performs information processing for the whole body. The mechanism of how the brain accomplishes its tasks are mostly unknown and full discovery of these mechanisms is the foundational purpose of neuroscience.

When information is being processed, small currents flowing in the active pyramidal cells (neurons) of the cerebral cortex of the brain thus, -producing electric and magnetic fields. Because of this electrical behavior, signs of neural activity in the brain can be measured with electrodes attached to the scalp or with very sensitive magnetic detectors placed near the scalp. The study of measuring and interpreting the electrical measurements from the scalp is called electroencephalography (EEG). The measurement of small potential differences at the scalp was first performed by Hans Berger (Berger, 1929). In his experiment, two large sheets of tinfoil were used to serve as electrodes, one in the forehead and one on the back of the head. Today, EEG with arrays of electrodes, is a clinical routine in brain research. The study of magnetic signals associated with the electric currents is called Magnetoencephalography (MEG) (Cohen, 1968; Hämäläinen et al., 1993). The weak magnetic fields outside the head due to currents in the brain are picked by a superconducting quantum interference device (SQUID), which is a sensitive detector of magnetic flux, introduced in the late 1960's by James Zimmerman (Zimmerman et al., 1970).

Many important technologies are available to image the human brain. Anatomical structures can be investigated by computer aided tomography (CT) scans and by magnetic resonance imaging (MRI). These methods provide high-quality images about the histology of the tissues. However, for acquiring metabolic information about the brain, other imaging methodologies are required. Brain activity can be measured with very good spatial accuracy using nuclear imaging methods such as positron-emission tomography (PET) (Jaszczak, 1988), single-photon emission tomography (SPECT) (Knoll, 1983) or functional magnetic resonance imaging (fMRI) (Belliveau et al., 1991), which reflect changes of the blood flow or oxygenation in the brain. The temporal resolution of PET is on the order of seconds or around 0.1 second at best. It is possible to acquire fMRI data within 100-ms intervals but properties of the blood flow in the brain practically limit the temporal resolution of this method to 1 s. Electromagnetic imaging modalities have a much better temporal resolution, which is around 1 ms for MEG. This is considerably better than in other modalities with a similar spatial resolution. In addition, a very important advantage of electromagnetic techniques is that they are completely *non-invasive*, whereas, in nuclear imaging techniques, limitations are imposed on the maximum radiation dosage in order to safeguard the individual under examination.

By using an array of electric and magnetic sensors, the cooperative activity of many areas of the brain are revealed in terms of complex signal patterns. Our task is then to interpret the complex patterns of the measured electric potential and magnetic field, in terms of the locations and time-course of the underlying sources. The key to this task is setting up a computational model that we can use to simulate the sources and the field patterns that represents the underlying activity. In order to achieve the most accurate representation of this activity, the model should incorporate a realistic geometry of the individual subject's head and realistic electrical conductivity information of the tissues associated with this geometry.

The calculation of the electric and magnetic field pattern for a given model of the human head is known as the *forward problem*. The calculation of the locations and time-course of the neural activities from the measured field patterns is called the *inverse problem*. In EEG or MEG studies, the simplest way to geometrically model the head is to use single sphere or concentric spherical shells each having homogeneous isotropic conductivity. The main reason behind employing sphere as a computational model is the availability of fast analytical algorithms to calculate the forward problem. Localization errors with spherical models are also well known. However the spherical approximation to model the head may not be sufficient for source localization. Using MRI, it is possible to procure better geometrical models for the head. Also, in most parts of the head, conductivity is known to be inhomogeneous and anisotropic. Numerical methods such as Boundary Element Method (BEM) and Finite Element Method (FEM) provide the flexibility of utilizing a realistic geometry and including detailed conductivity information into the computational model.

This work concentrates on developing accurate solutions of the forward problem using both the BEM and the FEM with an aim to establish an accurate basis for inverse problem calculations. In BEM, the surface is discretized with triangles; high-order isoparametric and planar elements are used on the surface of computation. The numerical results are then compared with analytical results. In FEM, the volume is discretized with tetrahedrons. The FEM formulation employs 2-form Whitney elements to represent the primary sources as an alternative to dipole sources. The use of FEM allows including of a more detailed conductivity information (such as conductivity anisotropy) into the model with an attempt to solve the forward problem with greater accuracy.

Chapter 2

EEG and MEG in brain research

2.1 Origin of signals

The origin of the electrical currents, and consequently the measured electrical potentials and magnetic fields lies in the specialized cells; neurons of the brain. The nervous system is made up of neurons and glia (or glial cells). Neurons are involved in the brain's fundamental functions; fast, organized information processing and communication. Glial cells are involved in support functions such as structure and repairing. There are approximately 10 times more glial cells than neurons.

The general shape of neurons is longer and thinner than other cells of the body. They transmit information and communicate with each other using a combination of chemical and electrical signals. Figure 2.1 shows a simplified picture of communication between three neurons. Neuron 2 receives a chemical input from neuron 1, which causes an electrical signal along its length and generates a chemical signal, which is transmitted to neuron 3. The chemical signals are in the form of neurotransmitters, which are released by one neuron and detected by another. The electrical signals are in the form of action potentials, which travel along neuronal axons. While neurons have a variety of shapes and sizes, the most general features are dendrites, which receive input from other neurons, a soma or cell body, and the axon, which conveys electrical information.

In the brain, each neuron influences and is influenced by many other neurons. An action potential occurs when inputs at a neuron are summed and the threshold is exceeded. When the action potential reaches the axon terminal of the neuron, it results in the release of neurotransmitter from the presynaptic membrane, which causes *postsynaptic potentials* (PSP).

Two types of PSP's can be classified. The Excitatory postsynaptic potential (E)PSP, causes a depolarization of the cell due to the arrival of action potentials at a synapse.

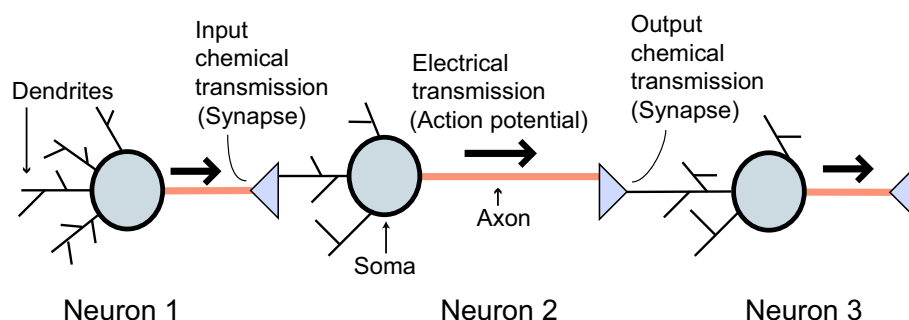


Figure 2.1: A simple picture of signal transmission in neurons.

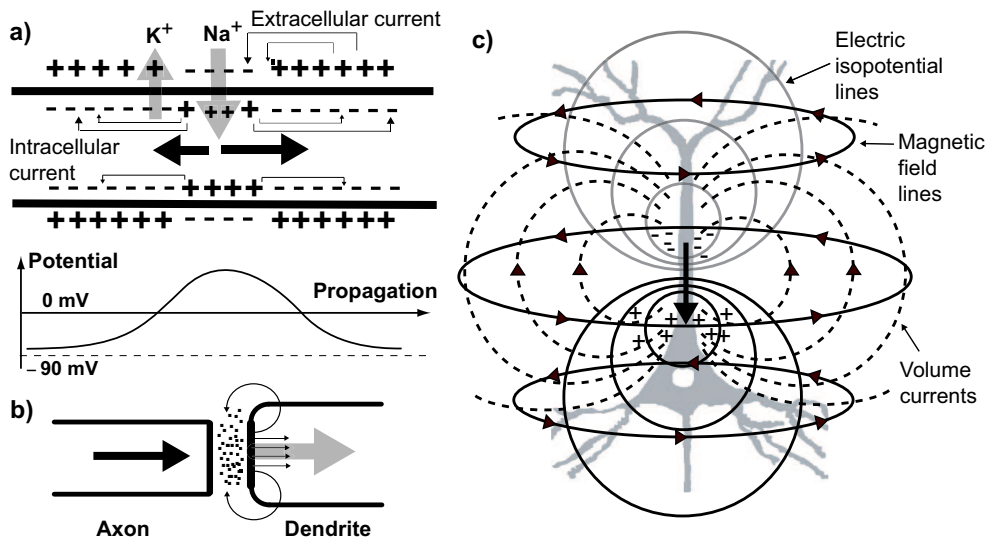


Figure 2.2: a) The Na^+ channels in the neuronal membrane open in response to a small depolarization of the membrane potential. The leading edge of the depolarization activates other nearby Na^+ channels and a wave of depolarization spreads from the point of initiation. Action potentials move in one direction. This is achieved because of the refractory period of the Na^+ channels. After activation Na^+ channels do not open again. This ensures that the action potential is propagated in only one direction along the axon. The intracellular current and oppositely directed extracellular current complete a closed circuit. Within the relatively long time during, which the current pattern develops (typically tens of milliseconds or more), it is reasonable to consider the intra- and extracellular current pattern as approximately *quasi-static* (Williamson, 1990). b) Generation of postsynaptic potential. The black arrow shows an action potential terminating at a synapse. Neurotransmitters are released, either causing an IPSP or an EPSP with the gray arrow showing an approximation of the macroscopic current. c) Potential and magnetic field pattern together with volume currents for an equivalent dipole as a primary source.

Once the transmembrane potential rises above a critical value, the cell triggers a new action potential. In the other case, the synaptic activation leads to a current of opposite sign causing a hyperpolarization of the postsynaptic neuron, this is called an inhibitory (IPSP).

2.2 Electrochemical reactions in neurons

Like any other biological cells, neurons have a membrane around them, which is selectively permeable to ions. Normally, the concentration of these ions such as potassium K^+ , chloride Cl^- and sodium Na^+ is different inside of the cell from that of the outside. In the resting state of a neuron, the Na^+ ion concentration is greater outside the cell than inside, whereas the opposite is true for K^+ ions.

In the resting state, the Na^+ - K^+ pump ejects Na^+ ions to out of the cell, against the high concentration of Na^+ outside of the cell in exchange for K^+ ions making the inside of the cell approximately 10 times richer in K^+ . The K^+ channels allow the K^+ ions adjacent to the membrane to leak out of the cell easily due to diffusion gradient. The permeability of the membrane to Na^+ ions is low in resting condition so there is no

counter flow of Na^+ from outside to inside. The K^+ outflow gives rise to a net shortage of positive charges inside the membrane compared to the outside. The result is that the inside of the cell has a more negative potential. The value of the potential is around -70 mV with respect to the outside of the cell. This is called the resting potential. Due to the thinness of the cell membrane (few nanometers) and potential difference around 70 mV, a large electric field is present on the order of 10^7 V/m across the cell membrane.

The resting electric field of the membrane is altered when responding to a stimulus, e.g. excitatory synaptic activity. The alteration induces a realignment of the channel dipole moment across the Na^+ channel, which changes the molecular conformation of the channel and in effect changes the state of the channel to be either open or closed. The change in permeability of the membrane to Na^+ allows a small influx of Na^+ into the cell leaving a local depletion of positive charge in the extracellular medium. When the depolarization reaches about -55 mV, the neuron fires an action potential and more Na^+ ions rush into the cell due to concentration gradient. This makes the inner side of the membrane more positively charged (depolarized) with a value of $+10$ to $+30$ mV, which lasts for about a millisecond. The process is terminated when the voltage reversal across the membrane drives the Na^+ channel into inactivated state and closed by inactivation. Subsequently, the K^+ channels open, allowing an outflow of potassium ions, which brings the membrane into resting state again. This chain of events enable the action potential to travel along the axon.

Current dipole

The action potential can be described by a quadrupole, whose magnetic and electric fields decay more rapidly than those of a dipole (Wikswo, 1983). The postsynaptic potential can be described by a *current dipole*, giving rise to currents in the surrounding tissues, which can exist for several tens of milliseconds causing the so called volume currents (Plonsey, 1981; Karp, 1981). Accordingly, while the MEG mainly records the magnetic field generated by the currents flowing in dendrites of the pyramidal neurons due to the PSP's (da Silva and van Rotterdam, 1987), the EEG records the potential due to volume currents flowing in brain as a result of the mentioned postsynaptic activity.

To represent the simplest kind of source, a current dipole is often used to explain the relationship between neuronal activity and the measured electric and magnetic fields. The current dipole is a point source, a mathematical abstraction to represent a short element of current. The dipole model, to represent the electrical properties of a biological source of current is usually satisfactory when a small region of active tissue is considered far from the measurement sensors. Moreover, the largest linear dimension of the active region should be much smaller than the distance from the source region to the measuring electrodes or magnetic field sensor. Assuming a current dipole as a source, figure 2.2c provides an illustration of the isopotential and magnetic field around the dipole.

2.3 The cerebral cortex

In EEG and MEG studies one is usually concerned with the uppermost layer of the brain; the cerebral cortex, which is 2–4 mm thick sheet of gray tissue where most of the measured neural activity takes place. The section of cortex is illustrated in figure 2.3.

At least 10 billion neurons reside in the whole cortex tissue. The total surface area of the cortex is about 2500 cm^2 , folded in a complicated way, so that it fits into the cranial cavity formed by the skull.

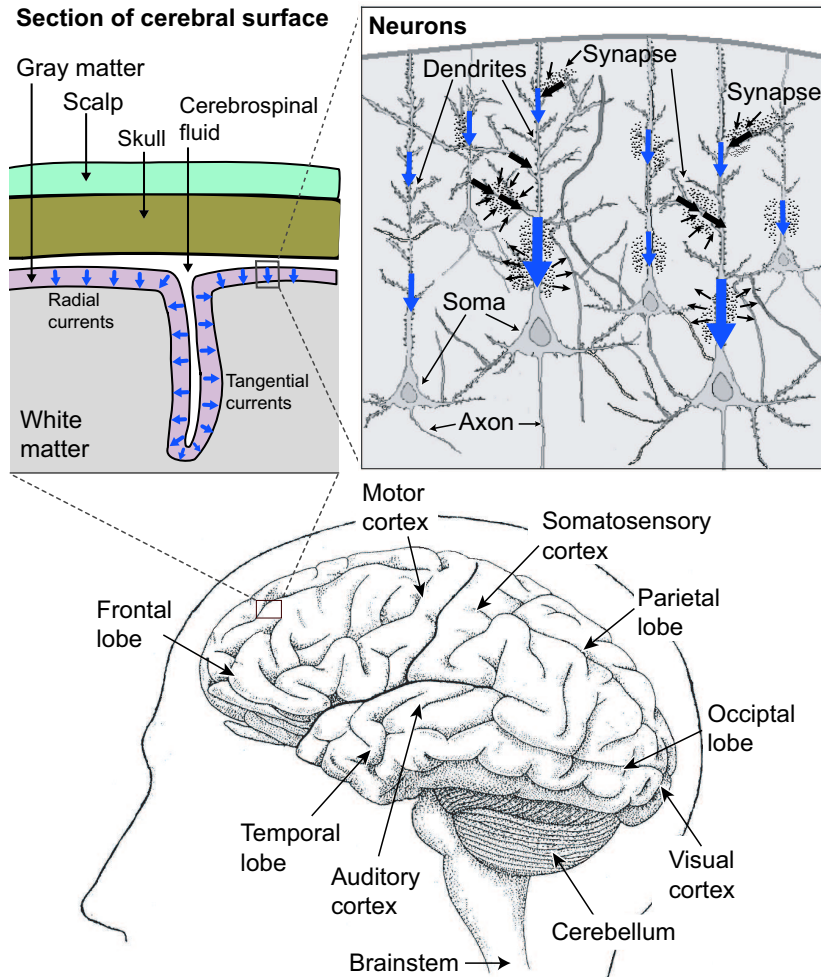


Figure 2.3: The orientation of the pyramidal neurons are such that they are normal to the cortex surface. Activation of excitatory synapses in the dendrites lead to postsynaptic potentials, which cause a convergence of ions in the apical dendrites. Synchronous activation of around 10^7 synapses can produce magnetic fields of 10 fT outside the skull. The produced magnetic field is a combination of the field generated by the primary postsynaptic currents and the field generated by the volume conductor currents in the extracellular space. MEG signals reflect the current flow in the apical dendrites of pyramidal cells oriented tangential to the skull surface. In effect, MEG is insensitive to radially oriented currents. EEG is sensitive to both tangential and radial source activity. Brain illustration adapted from (Hämäläinen et al., 1993).

Most regions of the cortex have mapped functionally. For example, the primary somatosensory cortex receives tactile stimuli from the skin. The area in the frontal lobe contains neurons concerned with integration of muscular activity. Primary motor cortex is involved in the movement of a specific part of the body. Large areas of cortex are devoted to body parts, which are most sensitive to touch (e.g. lips) or to the parts where accurate control of muscles is needed (e.g. fingers). The cortex is organized in layers parallel to the surface. Six layers can be distinguished.

Layer 1 is on the surface. Layers 2, 4 and 6 are populated with stellate cells, which have a star shaped form and cannot generate a substantial magnetic field. On the other hand, pyramidal cells, which are mainly located in layer 5, (Okada, 1981) have a linear structure with dendrites arranged parallel to each other and perpendicular to cortex surface, accordingly magnetic fields are generated when these cells are activated.

Activation of a single neuron does not cause a measurable electric or magnetic field. However, when an area of several mm^2 is excited almost synchronously, the electric and magnetic fields can be observed. It is estimated that 100,000 neurons are present within 1 mm^2 of cortical surface (Rockel et al., 1980). Half of this number are pyramidal cells, which are the main contributors of the measured electric and magnetic fields.

The true size of realistic current sources associated with brain activation varies according to the cause of the activation. Typically sensory stimuli activate cortical areas starting from a few mm^2 up to a few cm^2 , whereas for spontaneous activity and epileptic foci can involve an activation area up to tens of cm^2 . In MEG, a layer of activation around 2 cm in diameter cannot be distinguished from a point-like dipole (Okada, 1985; Hari et al., 1988).

2.4 Measuring bioelectromagnetic fields

When a sensory stimulus initially activates a small portion of the cortex, in addition to the primary current source due to cellular concentration gradients, passive ohmic currents are set up in the surrounding medium. This so called *volume current* completes the loop of ionic flow so there is no buildup of charge. As a result, the measured electric potential (EEG) and the magnetic field (MEG) are produced by both primary and volume currents. In both methods, the measured signals are generated by the same synchronized neuronal activity in the brain. An important aspect required to analyze the electric and/or magnetic data is developing mathematical and visualization techniques that utilize the collected data for characterizing the complex spatio-temporal patterns of activation.

2.4.1 EEG, the measure of bioelectric field

EEG measurements consists of recording a set of electric potential differences between pairs of scalp electrodes. These potential differences develop as a result of volume currents that spread from their source in active neural tissue throughout the conductive media of the head. The sensors are either glued to skin at locations directly above cortical regions of interest or placed on a flexible cap fitted to the head, with a uniform coverage of the scalp. State of the art EEG caps provide 256 electrodes for measurements.

EEG is a very successful clinical tool, especially in the study of epilepsy. Epileptic seizures are characterized by abnormal electrical behavior in neurons in affected regions. This abnormality produces large potential differences in the scalp, which can be easily observed with EEG. However, event-related signals (or evoked potentials) associated with the presentation of a sensory or cognitive stimulus cannot be distinguished from the background brain activity. Solution to this problem is averaging and recording of several stimulus-locked EEG traces (Dawson, 1947). Using this technique, spatio-temporal components of the EEG signal related with the stimulus are

revealed and background noise is reduced. A problem with this approach is; averaging of the signals often require the assumption that recorded signals are stationary, which does not always hold true especially in long time duration. New research approaches propose the study of between-trial variations in effect reducing the number of trials in the averaging process (Vigario and Oja, 2000), or analyzing of unaveraged EEG data (Karjalainen et al., 1999).

The major drawback in estimating cerebral sources from EEG recordings is the reported effect of variables such as thickness of the skull and scalp, conductivity anisotropy, and inhomogeneity of the head, on the forward problem solutions and source localizations. Earlier analysis of EEG based on model studies and measurements show that low conductivity of the skull spreads out the potentials in transverse directions (Williamson and Kaufman, 1983). As a result, focal sources in the brain could be averaged out in the scalp. Recent results show a decrease of potentials in the skull depending on its thickness (Chauveau et al., 2004). Holes in the skull also affect source localization (van den Broek, 1997; Oostenveld and Oostendorp, 2002).

2.4.2 MEG, the measure of biomagnetic field

EEG has been established as a method to evaluate functioning of the brain with clinical standing. However, application of neuromagnetic techniques during the past 20 years have proven the importance of MEG data in elucidating sensory, motor, and cognitive functions. MEG signals are associated with current flowing within the cortex, thus functional imaging of the brain with the help of studies of both ongoing spontaneous brain activity and event-related signals is possible. Brain currents can be measured as precisely as EEG but without physical contact of the sensors. This has the advantage of being easier both on the patient and the researcher since no electrodes need to be attached to the head making it possible to screen large numbers of patients quickly and easily.

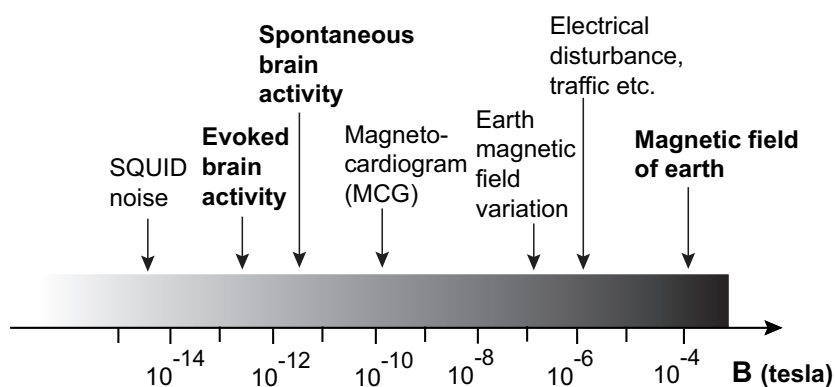


Figure 2.4: Magnetic field strengths on a scale.

The activity recorded in MEG is mostly confined to a frequency window less than 100 Hz but components up to 600 Hz have been studied (Haueisen et al., 2001). The strength of the biomagnetic field is 50–500 fT (Hämäläinen et al., 1993), which is about 10^9 times smaller than the magnetic field of the earth. Figure 2.4 shows the scale of magnitudes for different phenomena. The measurement of neuromagnetic fields are quite weak and require extremely sensitive sensors with a good control of the external noise.

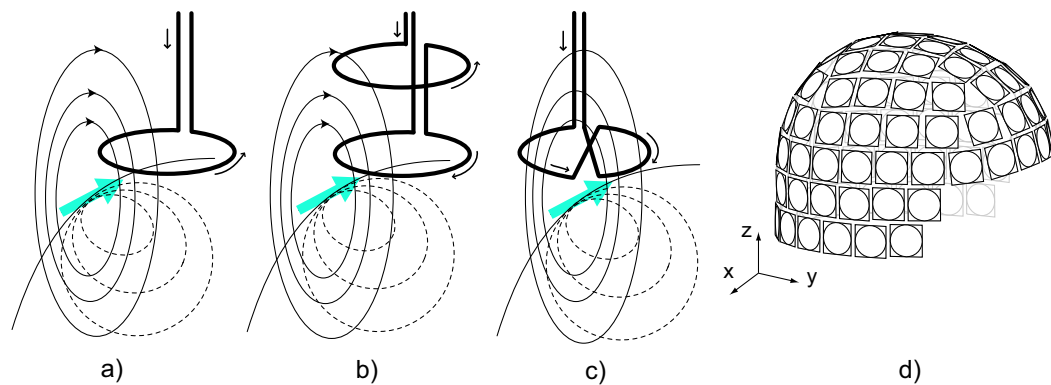


Figure 2.5: a) A magnetometer to measure magnetic field. b) First order axial gradiometer detects the z -derivative of the magnetic field and consists of two coils connected in series but wound in opposite senses, separated by a distance, baseline. c) A planar gradiometer detects the x and y derivatives of the magnetic field. d) The Neuromag VectorView™ helmet shaped measurement array for MEG consists of 102 magnetometers and 204 first order planar gradiometers.

The sensor used in biomagnetic instruments is called superconducting quantum interference device (SQUID), (Zimmerman et al., 1970). When cooled to very low temperatures, superconductors conduct electricity without resistance. This lack of resistance allows a SQUID to measure the interference of quantum-mechanical electron waves circulating in the superconducting loop as the magnetic flux enclosed by the loop changes and the SQUID circuitry produces a voltage proportional to this change. The associated computer software converts the SQUID data into current flow maps throughout the brain as a function of time. David Cohen was the first to record the brain activity using an induction coil magnetometer with 10^6 turns and a ferrite core (Cohen, 1968). Because the signal was very weak, the detected voltages were averaged by using a simultaneously measured EEG as a reference to bring the signal above noise level. Later, with improved shielding and a SQUID magnetometer, MEG results, comparable to that of EEG were obtained (Cohen, 1972).

Coil configuration

Coil configuration is an important factor in SQUID instruments. The simplest coil configuration for detecting changes in magnetic fields is a magnetometer. However, magnetometers are very sensitive to all signals in the environment. If we are interested in a very narrow area and the magnetic signal of interest is weak, the environmental magnetic interference could prevent useful signal measurement. In this case a gradiometer can be constructed. An axial or planar gradiometer reduces ambient magnetic field noise generated by relatively distant sources but still it is sensitive enough to tiny magnetic signals generated by a local source. The theory of gradiometer design utilizes the fact that uniform magnetic fields induce equal but opposite quantities of flux into two coils, which results in zero net flux in the gradiometer. On the other hand, magnetic signals in the vicinity that vary spatially along the length of the gradiometer produces a measurement that is proportional to the flux gradient.

While axial and planar configurations have the capability of reducing interference on the same level, they have different spatial sensitivity (Malmivuo and Plonsey, 1995). The axial gradiometers have circular (vortex like) sensitivity distribution concentrated

around the sensor loop. Planar gradiometers have linear distribution of sensitivity that varies with distance from the measurement plane. The maximum of the sensitivity and consequently the most likely location of the signal source is located directly under the symmetry axis of the planar gradiometer (Malmivuo et al., 1997). For source localization purposes, the use of either axial or the planar gradiometer configuration does not significantly affect the localization precision (Bruno and Romani, 1989; Mosher et al., 1997). Figure 2.5 shows different coil configurations. More detailed descriptions of the sensor design and interference suppression can be found, e.g. in (Hämäläinen et al., 1993), (Vrba and E.Robinson, 2001) and (Taulu et al., 2005).

Chapter 3

Theory and modeling of bioelectromagnetic fields

An important aspect required to analyze the electric and magnetic data obtained from EEG and MEG measurements is the development of mathematical and visualization techniques to analyze the complex spatio-temporal patterns of activation in the brain. The *inverse problem* involves estimation of the properties of the current sources within the brain that produced these signals. Before such an estimate is made, we must first solve *the forward problem*, where the scalp potentials and magnetic field for a known set of current sources representing neural activity is computed. If the primary source and the surrounding conductivity distribution are known, electric potential and the magnetic field can be calculated from Maxwell's equations.

3.1 Maxwell's equations

Let Ω be a general volume conductor of interest as shown in figure 3.1. The current density within Ω induces a magnetic field outside, which is observed at sensor locations $\mathbf{r}_1, \dots, \mathbf{r}_L$ and orientations $\alpha_1, \dots, \alpha_L$.

When the conductivity σ and the electric current generators are known, Maxwell's equations and the continuity equation $\nabla \cdot \mathbf{J} = -\partial\rho/\partial t$ can be used to calculate the electric field \mathbf{E} and the magnetic field \mathbf{B} ; where \mathbf{J} and ρ are the current density and charge density, respectively.

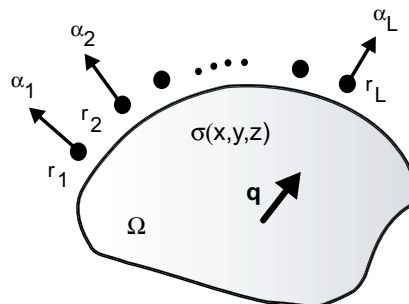


Figure 3.1: A focal current source represented by a current dipole \mathbf{q} in an inhomogeneous volume conductor Ω and surface $\partial\Omega$. The current dipole is defined by the primary current density \mathbf{J}_p in a differential volume element dv , i.e.; ($\mathbf{q} = \int \mathbf{J}_p dv$). The conductivity distribution is denoted by $\sigma(x, y, z)$.

Maxwell's equations for magnetic field intensity \mathbf{H} and electric field \mathbf{E} are,

$$\nabla \times \mathbf{H} = \frac{\partial \mathbf{D}}{\partial t} + \mathbf{J}, \quad (3.1)$$

$$\nabla \times \mathbf{E} = -\frac{\partial \mathbf{B}}{\partial t}, \quad (3.2)$$

$$\nabla \cdot \mathbf{B} = 0, \quad (3.3)$$

$$\nabla \cdot \mathbf{D} = \rho \quad (3.4)$$

with the constitutive relations between the field quantities specified as

$$\mathbf{D} = \epsilon \mathbf{E}, \quad (3.5)$$

$$\mathbf{B} = \mu \mathbf{H}, \quad (3.6)$$

$$\mathbf{J} = \sigma \mathbf{E}, \quad (3.7)$$

where the constitutive parameters ϵ, μ and σ denote permittivity, permeability and conductivity of the medium, respectively. These parameters are scalar for isotropic and tensors for anisotropic media.

3.1.1 Quasi-static approximation

If the effects of the time dependent terms in Maxwell's equations can be neglected, the solution of the equations would become simpler. Whether neglecting is allowed depends on the frequency of the signals and the properties of the medium, σ, ϵ, μ . The frequency of the signals obtained from bioelectromagnetic measurements in MEG and EEG are typically below 1 kHz. With this information it has been verified that the physics of MEG and EEG can be described by the *quasi-static* approximation of Maxwell's equations (Plonsey, 1969; Hämäläinen et al., 1993).

The terms with time dependency can be omitted and source terms in equation 3.1 and equation 3.2 can be written as

$$\nabla \times \mathbf{H} = \mathbf{J}, \quad (3.8)$$

$$\nabla \times \mathbf{E} = 0. \quad (3.9)$$

Let us denote the total current density produced by neuronal activity by \mathbf{J} . We can divide the current in two components,

$$\mathbf{J} = \mathbf{J}_p + \mathbf{J}_\Omega. \quad (3.10)$$

The \mathbf{J}_p is primary current and $\mathbf{J}_\Omega = \sigma \mathbf{E}$ is the volume current, which results from the effect of electric field on charge carriers in the conducting medium. Here σ is the macroscopic conductivity within Ω .

Taking the divergence of both sides of equation 3.8 we have

$$\nabla \cdot (\sigma \mathbf{E} + \mathbf{J}_p) = \nabla \cdot \mathbf{J} = 0. \quad (3.11)$$

Equation 3.11 represents our current model. Primary current is generated by neural activity within the neuronal cells whereas the volume currents flowing passively in the medium are caused by conduction effects. The total current is the sum of these two current components. The primary current represents the source of the brain activity

which we are trying to locate. In addition, modeling the volume currents enhances the localization accuracy.

Equation 3.9 can be satisfied by representing electric field \mathbf{E} with a gradient of a scalar function, the potential V as;

$$\mathbf{E} = -\nabla V, \quad (3.12)$$

The volume current can be written as

$$\mathbf{J}_\Omega = -\sigma \nabla V. \quad (3.13)$$

From the conservation of charge, $\nabla \cdot \mathbf{J} = 0$, along with the fact that no current flows out of the body, it follows that the electric potential solves the boundary value problem

$$\nabla \cdot \sigma \nabla V = \nabla \cdot \mathbf{J}_p, \quad \text{in } \Omega \quad (3.14)$$

$$\mathbf{n} \cdot \sigma \nabla V = 0, \quad \text{on } \partial\Omega. \quad (3.15)$$

If V is a solution of equations 3.14 and 3.15, then $V + c$, where c is a constant, also fulfills equation 3.14 and equation 3.15.

To derive partial differential equation for \mathbf{B} , we begin taking curl of equation 3.8,

$$\nabla \times (\nabla \times \mathbf{B}) = \mu_0 \nabla \times \mathbf{J}. \quad (3.16)$$

Here $\mathbf{J} = \mathbf{J}_p - \sigma \nabla V$ and μ_0 is the permittivity of free space. Using the vector relation $\nabla \times (\nabla \times \mathbf{B}) = \nabla(\nabla \cdot \mathbf{B}) - \nabla^2 \mathbf{B}$,

$$\nabla(\nabla \cdot \mathbf{B}) - \nabla^2 \mathbf{B} = \mu_0 \nabla \times \mathbf{J} \quad (3.17)$$

is obtained. Since $\nabla \cdot \mathbf{B} = 0$, we obtain the following

$$\nabla^2 \mathbf{B} = -\mu_0 \nabla \times \mathbf{J}, \quad (3.18)$$

$$\mathbf{B} = 0 \quad \text{at} \quad \infty. \quad (3.19)$$

Equation 3.18 is of Poisson's type. Analytical solutions can be found only for simple, specific geometries and conductivity distributions. Equation 3.19 is the boundary condition of \mathbf{B} .

3.2 Current dipole as a source model

The potential distribution and the measured magnetic field from the head are mainly generated by current sources due to the excitation of pyramidal neurons (da Silva and van Rotterdam, 1987). These current sources cannot be directly determined but rather derived from observations with some assumptions. The inverse problem, i.e., the determination of sources from the observed potentials and magnetic field, does not have a unique solution. Infinitely many configurations of sources can generate the observed potential and magnetic field patterns. The inability to solve this problem was already shown (Helmholtz, 1853). A way to bypass this limitation is to make an approximation of the sources, create an assumed equivalent source model to describe the sources with specific parameters on the basis of observed potential and magnetic fields.

At distances further away than size of the source region, the primary current source can be approximated by the current dipole,

$$\mathbf{J}_p(\mathbf{r}) = \mathbf{q}\delta(\mathbf{r} - \mathbf{r}'), \quad (3.20)$$

where $\delta(\mathbf{r} - \mathbf{r}')$ is the Dirac delta function evaluated at \mathbf{r}' and \mathbf{q} is the dipole moment.

In the general case of a distribution of neural activity, from the superposition principle, the resulting electric potential and magnetic field patterns can be viewed as arising from a distribution of current dipoles within the active area. The field and potential are the sums of the contributions from these individual dipoles. Therefore, the solutions to be concluded on using a single dipole model can be generalized to cases with multiple sources.

3.3 Volume conductor models

The forward problem, i.e., calculating magnetic fields and potentials at the measurement locations with a given source distribution is well-posed (Nunez, 1981). Although this is a solvable problem, in practice, approximate solutions need to be used in the calculation due to the fact that the volume conductor characteristics are usually not known in detail. For this reason, a simplified model of the electrical conductivity characteristics of the head is set up for the solution. Table 3.1 shows a comparison of the capabilities of various methods that can be used in the forward problem solution. Using different solution methods, with volume conductors of varying complexity that model the head, solution methods can be compared and analyzed for their inherent errors and new methods can be validated.

Table 3.1: Computational methods to solve the forward problem for various models of the head. The solution of Poisson's equation for infinite medium for V and \mathbf{B} is given in section 3.3.1. The multiple spheres model described in section 3.4.4 provides closed form solutions for single and multiple layer spherical head model. The numerical methods BEM and FEM are described in chapter 4. The letters H, NH, I, A describe the conductivity structure of the models and defined as; H=Homogeneous, NH=Inhomogeneous, I=Isotropic, A=Anisotropic. *Although BEM can handle anisotropy (Zhou and van Oosterom, 1994; Tonon et al., 2000) it is not convenient to use in neuromagnetism due to the fact that interfaces of different conductivity, abundant in the head, require careful consideration.

Computable Model	Direct Poisson	Multiple Spheres	BEM	FEM
Infinite H, I	✓	×	×	×
Single Sphere H, I	×	✓	✓	✓
Multiple Spheres H, I	×	✓	✓	✓
Multiple Spheres H, A	×	✓	×*	✓
Realistic H, I	×	×	✓	✓
Realistic NH, A	×	×	×*	✓

3.3.1 B and V for infinite volume conductor

For localization of the electrical activity in the brain, an infinite volume conductor with homogeneous and isotropic conductivity is an over-simplified geometric model. However, the expression for an infinite volume conductor is quite important. The electrical potentials and magnetic fields of more complicated volume conductor models with multiple conductivity interfaces are usually computed in such a way that final solution can be obtained by adding geometrical correction terms to the infinite volume conductor solution. With this mathematical application, the solution is smoothed with respect to the field singularity at the source locations.

The Poisson equation for the potential in an infinite homogeneous volume conductor with constant scalar conductivity σ is

$$\sigma \nabla^2 V(\mathbf{r}) = \nabla \cdot \mathbf{J}_p. \quad (3.21)$$

The potential due to a current density can be found with

$$V(\mathbf{r}) = \frac{1}{4\pi\sigma} \int_{\Omega} \mathbf{J}_p(\mathbf{r}') \cdot \frac{\mathbf{r} - \mathbf{r}'}{|\mathbf{r} - \mathbf{r}'|^3} d\Omega, \quad (3.22)$$

which reduces to

$$V_0(\mathbf{r}) = \frac{1}{4\pi\sigma} \frac{\mathbf{q} \cdot \mathbf{R}}{R^3}, \quad (3.23)$$

for a current dipole $\mathbf{q}(\mathbf{r}')$ where $\mathbf{R} = \mathbf{r} - \mathbf{r}'$, $R = |\mathbf{r} - \mathbf{r}'|$.

The magnetic field due to a current density \mathbf{J} in a homogeneous infinite volume conductor is obtained using the Biot-Savart (Ampere-Laplace) law:

$$\mathbf{B}(\mathbf{r}) = \frac{\mu_0}{4\pi} \int_{\Omega} \mathbf{J}_p(\mathbf{r}') \times \frac{\mathbf{r} - \mathbf{r}'}{|\mathbf{r} - \mathbf{r}'|^3} d\Omega. \quad (3.24)$$

The integration is performed over the volume containing the current sources. For a current dipole $\mathbf{q}(\mathbf{r}')$, this reduces to

$$B_0(\mathbf{r}) = \frac{\mu_0}{4\pi} \frac{\mathbf{q} \times \mathbf{R}}{R^3}. \quad (3.25)$$

In an infinite homogeneous volume conductor, the volume currents do not contribute to the electric potential or the magnetic field (Plonsey, 1981). The fields are only caused by primary currents \mathbf{J}_p . The magnetic field arises from the curl $\nabla \times \mathbf{J}_p$ and the electric potential from the divergence $\nabla \cdot \mathbf{J}_p$. The curl and divergence operators acting on \mathbf{J}_p are mathematically independent and similarly the electric potential and the magnetic field should also be independent. However this is not the case for conductor models, which are not of infinite extent. While the primary current stays the same, the interfaces of different conductivity act as secondary sources affecting the potential and magnetic field at different locations.

3.3.2 B and V for piecewise homogeneous conductor

The biological volume conductor consists of not one but many layers of tissue with different conductivity. The solution for \mathbf{B} given in equation 3.18 is,

$$\mathbf{B}(\mathbf{r}) = \frac{\mu_0}{4\pi} \int_{\Omega} \mathbf{J}_p(\mathbf{r}') \times \frac{\mathbf{r} - \mathbf{r}'}{|\mathbf{r} - \mathbf{r}'|^3} d\Omega' - \int_{\partial\Omega} \sigma(\mathbf{r}') \nabla V(\mathbf{r}') \times \frac{\mathbf{r} - \mathbf{r}'}{|\mathbf{r} - \mathbf{r}'|^3} d\Omega' \quad (3.26)$$

Here, \mathbf{r} is the point where the field is computed and the primed symbols refer to the source location. The integration is carried out over the head (Ω), and all variables inside the integral depend on source location inside the head. Equation 3.26 can be simplified by assuming the head to be a piecewise homogeneous, linear isotropic medium, also called a simple medium. Such a medium consists of several regions, each with a constant conductivity. Such a model is called a compartment model of the head.

By applying the Gauss theorem, $\int_G \nabla \times \mathbf{u} dv = \int_S \mathbf{u} \times d\mathbf{S}$, we can arrive at the formula for \mathbf{B} (Geselowitz, 1970; Hämmäläinen and Sarvas, 1989),

$$\mathbf{B}(\mathbf{r}) = \mathbf{B}_0(\mathbf{r}) + \frac{\mu_o}{4\pi} \sum_{k=1}^m \int_{S_k} \Delta\sigma_k V(\mathbf{r}') \frac{\mathbf{R}}{R^3} \times \mathbf{n} dS'_k. \quad (3.27)$$

where $\mathbf{R} = \mathbf{r} - \mathbf{r}'$ and $R = |\mathbf{r} - \mathbf{r}'|$. In these formulations \mathbf{r} and \mathbf{r}' are the measurement and source locations respectively. The term \mathbf{B}_0 is equal to the first term on the right hand side of equation 3.26 and denotes the contribution of the primary current, k denotes the number of the region over which the integration takes place, where it is a surface integration over the region and \mathbf{n} is normal to the surface. As can be seen from equation 3.27, the magnetic flux density depends on the potential at each surface.

An equation for the electric potential is (Geselowitz, 1967; Hämmäläinen et al., 1993),

$$\sigma(\mathbf{r})V(\mathbf{r}) = \sigma_0 V_0(\mathbf{r}) - \frac{1}{4\pi} \sum_{k=1}^m \int_{S_k} \Delta\sigma_k V(\mathbf{r}') \frac{\mathbf{R}}{R^3} \cdot \mathbf{n} dS'_k, \quad (3.28)$$

where S_k is the surface of the k^{th} homogeneous conductive region, and $\Delta\sigma_k$ is the difference of conductivity across the boundary of the k^{th} conductivity region in the direction of $d\mathbf{S}_k$, i.e., $\Delta\sigma_k = \sigma_k^- - \sigma_k^+$ where σ_k^+ denotes the electrical conductivity on the outside of the k^{th} boundary and σ_k^- denotes the electrical conductivity on the inner side of that boundary.

The first term in equation 3.28 gives the potential distribution when the region is unbounded. The second term is the effect of secondary sources at the conductivity interfaces. In a simple multilayered head model, the scalp, skull and brain are the major tissue types that produce conductivity interfaces (Rush and Driscoll, 1969). In studies for magnetic measurements, the effects of outer layers can be ignored and the head model can be constructed as a homogeneous brain shaped volume conductor (Hämmäläinen and Sarvas, 1989; Mosher et al., 1992; Ahonen et al., 1993), to simplify the computational procedure. However, in this approach the effect of the low conductivity of the skull, which is necessary for potential calculations is not taken into account.

It is worthwhile to note that equations 3.28 and 3.27 are only valid for conductors with closed homogeneous and isotropic compartments. In order to solve the forward problem numerically, the integral over the surface of a compartment must be discretized. Surface elements, for example triangles, are the basis of BEM. If conductivity anisotropy inside the volume conductor has to be taken into account, the volume integral must be discretized and solved numerically. In this case, the appropriate method is FEM, which has been also employed in the forward problem solution for the head (Yan et al., 1991; Thevenet et al., 1991; Awada et al., 1997; Haueisen et al., 1997; Wolters, 2003).

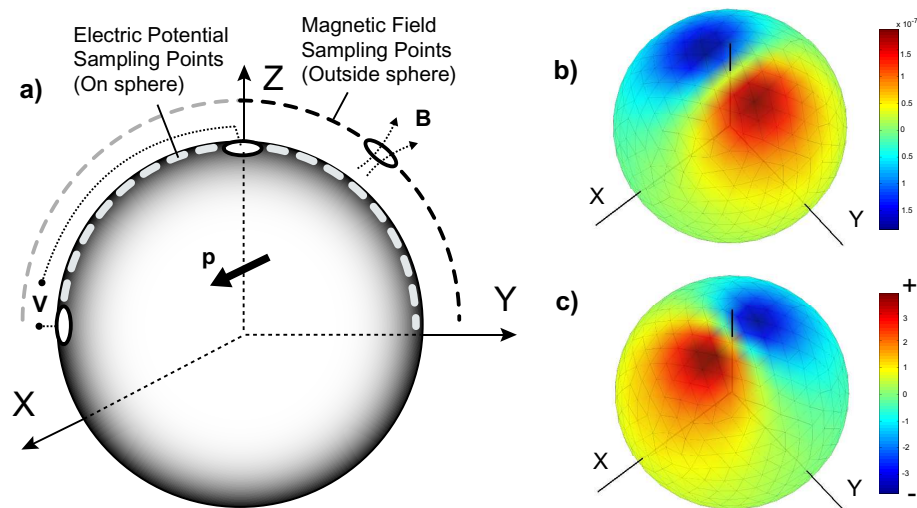


Figure 3.2: a) A current dipole \mathbf{p} in a homogeneous sphere with unit radius. The outer points just outside the sphere denote field points for the calculation of the magnetic field. The points on the surface of sphere are the field points where the electric potential is calculated. b) Magnetic field calculated for the configuration shown in figure a) with dipole coordinates $(0, 0, 0.60)$, dipole moment $(1, 0, 0)$ and unit conductivity. c) Electric potential for the same dipole.

3.4 Modeling the head

The head model is an important parameter in EMSI studies. In the earliest studies, head models with simple geometries and homogeneous parameters were used, permitting many simplifications in the computation. When using models with spherical symmetry, solving the forward problem can be reduced to evaluating an analytic expression. This drastically reduces the time to obtain a solution. On the other hand, realistic models can be constructed from complex shapes. Also detailed parameter information such as conductivity anisotropy can be assigned to different parts of the model. In this case, the closed form solutions cannot be easily found and numerical techniques such as BEM and FEM must be used.

3.4.1 Single sphere model

Early studies in EEG source modeling used a single sphere with homogeneous conductivity to represent the head (Wilson and Bayley, 1950; Frank, 1952; Geisler and Gerstein, 1961; Brody et al., 1973; Cuffin, 1978; Ary et al., 1981; Stok, 1986; He et al., 1987; Janday and Swithenby, 1987; Srebro et al., 1993; Berg and Scherg, 1994; Yao, 2000). For MEG, single sphere model to represent the inner surface of the skull is usually used.

Figure 3.2 shows this most basic kind of model to represent the human head used in source localization studies. The electric potential and magnetic field pattern due to the dipole is also shown. The studies using the single sphere model revealed that the single sphere model with homogeneous conductivity would produce large localization errors because it does not account for the *smearing* effect of the skull's low conductivity on scalp EEG's. The source localization accuracy with MEG does not suffer very much because the tissue conductivity does not alter the primary magnetic field.

3.4.2 Multiple spheres model

The advanced form of the spherical model consists of multiple number of spheres to represent layers of different conductivity. This mainly benefits EEG source analysis since including multi-layer conductivity information into the model reflects the actual composition tissue of conductivity much better. Volume conductor models of arbitrary number of layers have been prepared and used in many studies. Among these, the 3-layer (Rush and Driscoll, 1968, 1969; Cuffin and Cohen, 1977; Stok, 1986; Salu et al., 1990; Berg and Scherg, 1994) and 4-layer concentric shell models are mostly used in the literature (Cuffin, 1991; Zhou and van Oosterom, 1992; de Munck, 1988, 1993; Zhang, 1995; Sun, 1997) because of their good balance in simplification and representation of head parameters and availability of rapidly computable closed form expressions. Also a 5-layer model was studied (Uitert et al., 2002). The 3-layer model consists of three concentric spherical surfaces representing brain, skull and scalp tissue (Rush and Driscoll, 1969). This model has been checked experimentally in a saline-filled skull and has been shown to yield good semi-quantitative agreement with a variety of general observations of EEG (Nunez, 1981, 1990). The model was also used to observe the fields associated with dipolar sources (Cuffin et al., 1990). It was observed that a change in the thickness of scalp and skull layers produces differences on the calculated electric potential and magnetic fields. The conclusion was that variations in skull and scalp thickness would cause localization errors of less than 1 cm for inverse solutions using EEG's and much smaller errors for solution using MEG's.

Figure 3.3 shows this most basic kind of model to represent the human head used in source localization studies.

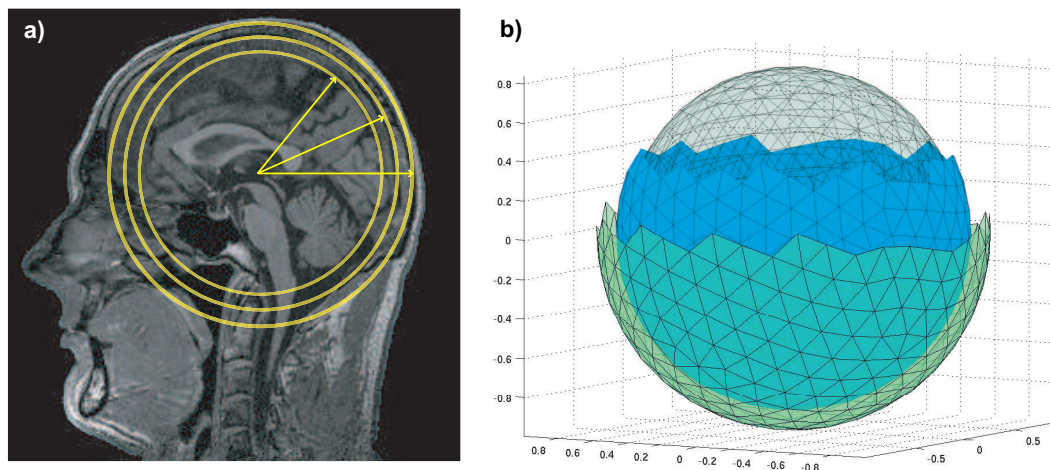


Figure 3.3: a) The three layer concentric spheres approximation imposed on an MRI image of the head. b) The BEM computational model for the three layer concentric spheres representation.

3.4.3 Realistic Head Models

Apart from using spheres to model the head, realistic head models for source localization have also been used (Hämäläinen and Sarvas, 1989; Hämäläinen et al., 1993; Wieringa, 1993; Zanow and Peters, 1995; Cuffin, 1996; Zanow, 1997; Leahy et al., 1998; Fuchs et al., 2001; Kaneko et al., 2001; Wagner and Fuchs, 2001; Vanrumste, 2001; Fuchs et al., 2002; Uitert et al., 2003). Magnetic resonance imaging enables

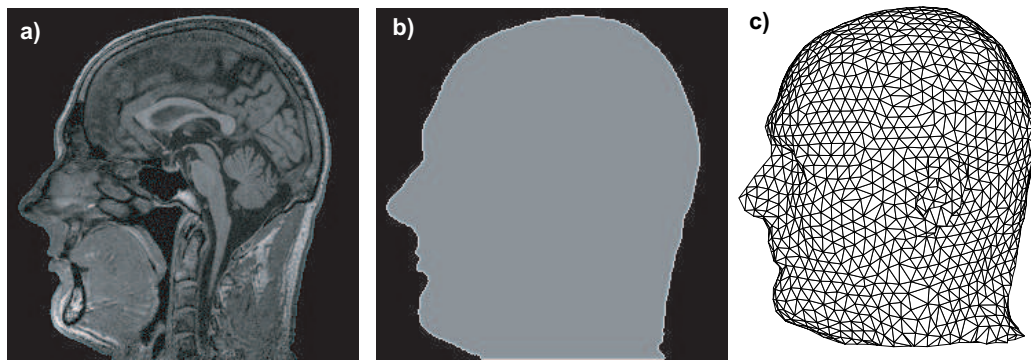


Figure 3.4: a) MR image of the head to be modeled. b) The surface segmentation of the MR image to prepare the computational model for BEM studies. c) The realistic BEM model is a triangular mesh of the surface, ready to be used in numerical calculations. Similarly realistic models for other parts of the head such as brain and skull can be created.

us to reconstruct a three dimensional model of the head that can be used in source modeling (Wieringa, 1993; Lötjönen et al., 1998; Koikkalainen and Lötjönen, 2004). Together with the realistic model and the source locations found using EEG/MEG, we can obtain functional information associated with the anatomical structure. Realistic models improve the accuracy of the forward problem solution. However, the forward problem must be solved numerically for arbitrary head shapes since analytical solutions are not available for arbitrary conductor geometries. In this case, the numerical techniques, FEM and BEM, can be used.

Non-spherical head shape can produce significant changes in the maps produced by some sources in the cortical region of brain (Cuffin et al., 1990; Cuffin, 1990). Such deviations of the head from sphericity produced localization errors of less than approximately 1 cm. Effects of local variations in skull and scalp thickness on EEG's and MEG's (Cuffin, 1993) and effects of using realistic head models (Cuffin, 1996) were also investigated. It was found that these variations affect EEG's and MEG's and together with changes in source depth and orientation in the localization. A similar study was done (Eshel et al., 1995) on correlation between skull thickness asymmetry and scalp potentials estimated by a 3-layer concentric sphere model of head. It was concluded that skull thickness asymmetry can create non-negligible asymmetries in the potential measured on the scalp above homotopic points of the two hemispheres. Numerical studies with BEM using a realistic head shaped model also suggest that the sphere model is not accurate enough for computing the magnetic fields of deep sources or sources near the bottom of the skull in fronto-temporal and frontal areas (Hämäläinen and Sarvas, 1989). In this case, using of a brain shaped homogeneous conductor model is suggested. In another simulation study (Ding and Y. Lai, 2005), BEM with LORETA for source localization was used. It was found that, using realistic head models with BEM eliminates localization errors caused by the spherical approximation and reduces the errors from 20-30 mm in the approximated spherical head model to about 10 mm in the realistic geometry head model. The results suggest that increase of localization accuracy may be achieved using the realistic geometry BEM head model compared to the spherical head model. In a study with realistic head model (Uitert et al., 2003) the importance of using realistic head models rather than spherical models, for forward and inverse MEG simulations was investigated. FEM

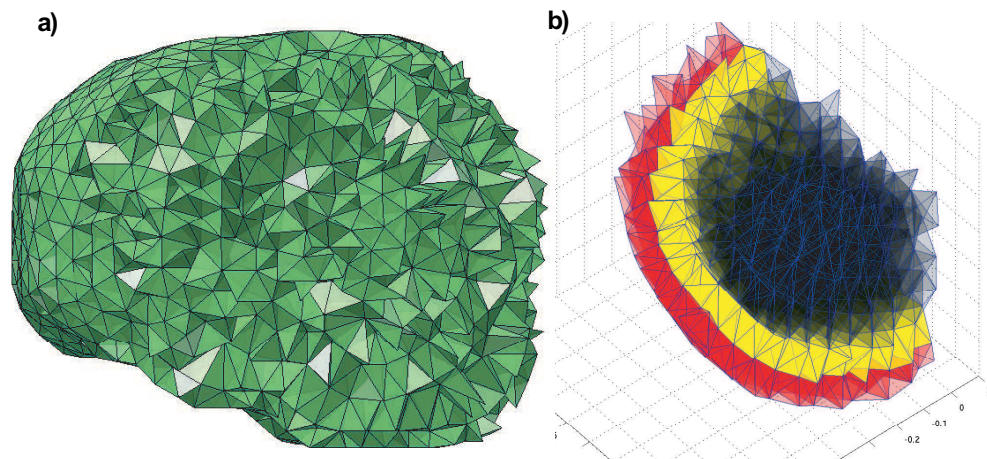


Figure 3.5: a) Realistic FEM mesh of the brain composed of tetrahedral elements. b) Each tetrahedron in the mesh can be tagged and assigned with a specific property such as a conductivity. Different colors help the visualization.

was used in the numerical simulations. It is concluded that for realistic head models the volume currents cannot be automatically disregarded like it is done for spherical models. The volume currents do affect the magnetic field measured by MEG on the human head and in realistic inhomogeneous head models. Including the magnetic field due to volume currents gives more accurate solutions to the EEG-MEG forward problem and helps to more precisely localize neural sources.

Segmentation: A Crucial step

Segmentation is the process of separating regions in an image. In order to obtain realistic models of the head, different tissue types from MR images have to be classified. The objective is to obtain a numerical model of the human head based on the geometry information and electrical properties of the classified tissues. This is achieved in three steps: segmentation, labeling and surface reconstruction. Segmentation provides a discrete 3-D set of data that belong to a specific tissue and labeling identifies the tissue type. As a final process, a surface reconstruction algorithm provides a list of polygons and vertices to represent the surface of the tissue. Segmenting tissues automatically from MR images is a difficult task because of the complexity of the tissue structures in the brain, variable imaging conditions, noise, the partial volume effect where one voxel contains more than one type of tissue. Numerous algorithms have been generated for image segmentation is discussed in literature (Haralick and Shapiro, 1985; Pal and Pal, 1993; Ayache, 1997) from low level techniques such as intensity and boundary based segmentation (Wells et al., 1995) to pattern recognition methods (Chunlin et al., 1993; Yan and Karp, 1995), neural networks (Hall et al., 1992; Bezdek et al., 1993; Wang et al., 1998), deformable models (Kass et al., 1987; Poon et al., 1994; Snell, 1995; Tek and Kimia, 1995; Yezzi et al., 1997; Lötjönen et al., 1999) and atlas based warping algorithms (Thompson and Toga, 1996; Sandor and Leahy, 1997).

3.4.4 Closed form solutions for B and V

The electric potential and magnetic field distribution, due to a current dipole in a volume conductor can be computed using closed form expressions for simple geometries, e.g., sphere. In applications, one is usually interested in the solution of electric potential at the surface of the volume conductor and magnetic field distribution outside the conductor, since measurements are done in those regions.

The Magnetic field

The magnetic field due to a dipole source $\mathbf{j}^p(\mathbf{r}) = \mathbf{q}\delta(\mathbf{r} - \mathbf{r}_s)$ inside a spherically symmetric conductor can be calculated using the formula (Sarvas, 1987):

$$\mathbf{b}(\mathbf{r}) = \frac{\mu_0}{4\pi F^2} (F\mathbf{q} \times \mathbf{r}_s - \mathbf{q} \times \mathbf{r}_s \cdot \mathbf{r} \nabla F), \quad (3.29)$$

where $\mathbf{a} = \mathbf{r} - \mathbf{r}_s$, $a = |\mathbf{a}|$, $r = |\mathbf{r}|$, $F = a(ra + r^2 - \mathbf{r}_s \cdot \mathbf{r})$ and $\nabla F = (r^{-1}a^2 + a^{-1}\mathbf{a} \cdot \mathbf{r} + 2a + 2r)\mathbf{r} - (a + 2r + a^{-1}\mathbf{a} \cdot \mathbf{r})\mathbf{r}_s$. Here \mathbf{q} is the dipole moment, the vectors \mathbf{r} and \mathbf{r}_s denote the *location of field* and *source points* respectively.

Electric Potential for a single sphere

In the case of a dipole inside a sphere with homogeneous, isotropic conductivity (Yao, 2000), the potential on the surface of the sphere due to a dipole at \mathbf{r}_s can be calculated as:

$$\begin{aligned} \phi(\mathbf{r}) = & \frac{1}{2\pi\sigma} \frac{\mathbf{q} \cdot (\mathbf{r} - \mathbf{r}_s)}{r_p^3} \\ & + \frac{1}{4\pi\sigma} \frac{1}{|r|^2} \left[r_p(\mathbf{q} \cdot \mathbf{r}) \right. \\ & \left. + \frac{\mathbf{q} \cdot \mathbf{r} |\mathbf{r}_s| \cos(\theta) - \mathbf{q} \cdot \mathbf{r}_s |\mathbf{r}|}{|\mathbf{r}| + r_p - |\mathbf{r}_s| \cos(\theta)} \right]. \end{aligned} \quad (3.30)$$

Here r_p is the length of displacement given by $r_p = \sqrt{|\mathbf{r}^2| + |\mathbf{r}_s^2| - 2|\mathbf{r}||\mathbf{r}_s| \cos(\theta)}$ and $\cos(\theta) = \mathbf{r} \cdot \mathbf{r}_s / |\mathbf{r}||\mathbf{r}_s|$. The conductivity of the isotropic and homogeneous sphere is represented by σ .

Anisotropic electric potential for multiple spheres

In the case of a dipole inside a multiple-spheres with anisotropic conductivity the potential on the surface of the sphere due to a dipole inside the innermost layer can be calculated (Zhou and van Oosterom, 1992; Zhang, 1995). The anisotropic means, in each layer the radial conductivity may be different from the tangential conductivity, but both are constant. A dipole with moment \mathbf{q} is located at \mathbf{r}_0 within the innermost sphere. The potential at \mathbf{r}_f for N-layer sphere is given by;

$$\begin{aligned} V(\mathbf{r}_f) = & \frac{q}{4\pi\sigma_N r_f^2} \sum_{n=1}^{\infty} \frac{2n+1}{n} \left(\frac{r_0}{r_f}\right)^{n-1} \\ & \times [f_n n \cos \alpha P_n(\cos \gamma) + g_n \cos \beta \sin \alpha P_n^1(\cos \gamma)]. \end{aligned} \quad (3.31)$$

Here α is the angle between dipole location \mathbf{r}_0 and dipole moment \mathbf{q} . γ is the angle between \mathbf{r}_0 and the measurement point \mathbf{r}_f . A plane P1 is defined by \mathbf{r}_0 and \mathbf{q} and

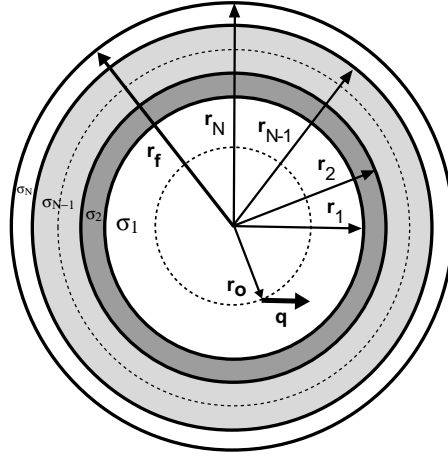


Figure 3.6: Illustration of a sphere with N -layers. The potential is calculated at r_f due to a dipole located at r_0 with moment q . The dipole is free to move inside the innermost sphere.

another plane P2 is defined by \mathbf{r}_0 and \mathbf{r}_f . β is the angle between P1 and P2. The terms P_n and P_n^1 represent the Legendre and the associated Legendre polynomials, respectively. The anisotropy information is embedded in the terms f_n and g_n . Open forms of f_n and g_n can be found in (Zhang, 1995).

The equation 3.31 can also be used to calculate potentials for multiple spheres with isotropic conductivity (Zhang, 1995). If the sphere is one-layer homogeneous, the potential can be calculated by setting $f_n = 1$ and $g_n = 1$ in equation 3.31 as;

$$V(\mathbf{r}_f) = \frac{q}{4\pi\sigma_N r_f^2} \sum_{n=1}^{\infty} \frac{2n+1}{n} \left(\frac{r_0}{r_f}\right)^{n-1} \times [n \cos \alpha P_n(\cos \gamma) + \cos \beta \sin \alpha P_n^1(\cos \gamma)]. \quad (3.32)$$

Figure 3.6 shows N -layer concentric sphere with the computation parameters given in equation 3.31.

Chapter 4

Numerical solution of the forward problem

In this chapter new formulations of Boundary Element Method (BEM) (Publication P2) and Finite Element Method (FEM) (Publication P5) are used to solve the Poisson's type equations for the electric potential V and the magnetic field \mathbf{B} . In order to numerically solve the integral equations, the computational domain is discretized by dividing it into simple elements. The unknowns are represented by known basis functions defined on these elements. The continuous integral equation is converted into a linear equation system by taking a scalar product with test functions. In publication P2 the collocation method with high order isoparametric elements was used. In the collocation method the space of the test functions is chosen to be the set of Dirac delta functions centered at each collocation point. This yields a number of collocation equations to be solved. In the Galerkin method the spaces of test functions and basis functions are the same. The basis functions in turn can be expressed as linear combinations of polynomial nodal shape functions of arbitrary degree. BEM is a suitable technique for piecewise homogeneous volume conductors (P1–P4). If detailed nonhomogeneous and anisotropic conductivity information is available, FEM (P1,P3,P5,P6) can be used. The 3D problem domain is partitioned into small volume elements where particular properties can be assigned for each element.

4.1 BEM with isoparametric elements, (P2)

In BEM, Green's theorem is used to transform the differential equations valid over a volume conductor into integral equations over boundary surfaces, which are present within the volume conductor. Thus, it is especially a suitable technique to calculate surface potentials, generated by current sources located in a piecewise homogeneous volume conductor. The effects of the primary current source at the boundaries of different regions conductivity within the volume, and the outer surface are calculated for the solution.

For this study, the human head is assumed as a piecewise homogeneous conductor; the BEM is used to approximate each boundary surface such as brain, cerebrospinal fluid, skull and scalp using small surface elements. The original integral equation governing surface potentials is approximated as a summation of surface integrals over each element. The potential on each element is first assumed as a linear function of node potentials (quadratic and cubic variations are also studied). After choosing the interpolation functions and element geometry, the surface integral over each element is expressed in terms of unknown node potentials, and the original surface integral

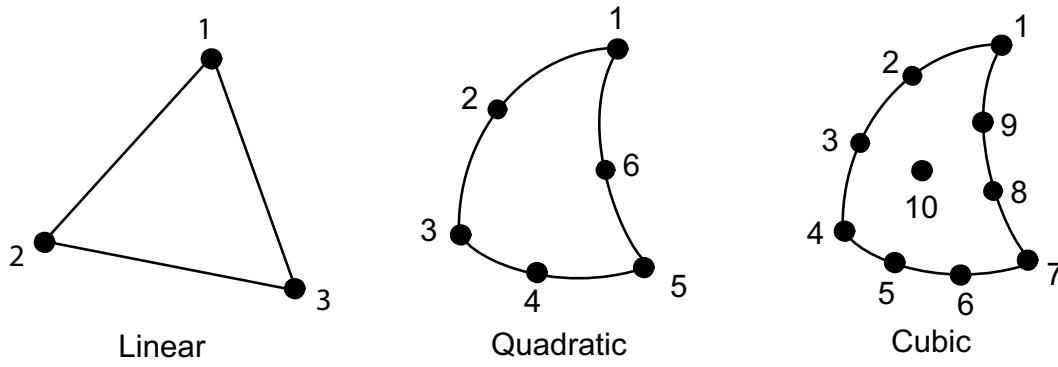


Figure 4.1: Isoparametric elements used in BEM calculations. 3 node linear, 6 node quadratic and 10 node cubic element.

is reduced to a system of algebraic equations. The solution of the node potentials provides the potential at any point on the surfaces (Tanzer and Gençer, 1997). The elements can have various shapes such as triangles or rectangles.

4.1.1 Triangular isoparametric surface elements

The isoparametric formulation in BEM employs triangular elements with linear, quadratic and cubic interpolation functions. Figure 4.1 shows typical surface element types. Isoparametric means that both variation in the geometry and the potential distribution on the element are defined with the same interpolation functions. Using isoparametric elements provides two advantages:

1. For higher order elements, the element sides can follow quadratic or cubic variations in geometry and function represented. So quite complicated physical geometries and functions can be represented with such elements,
2. Greater accuracy can be achieved by using fewer number of complex elements instead of a large number of simple elements.

The human cortex is a complex structure with folds and fissures, however the skull is relatively smooth with less complicated boundaries. It could be quite resource intensive in computational terms to model the cortex using BEM, due to the large number of folds of the cortex and the number of finite elements required to discretize the folds. However, it seems viable to model the inner part of the skull using isoparametric elements in BEM.

4.1.2 Implementation of the isoparametric BEM formulation

Let the interfaces between the regions of different conductivity be denoted by S_1, \dots, S_m with S_1 surrounding all other surfaces, i.e assume S_1 is the surface of the scalp. The electric potential V at $\mathbf{r} \in S_i$ obeys the integral equation

$$(\sigma_i^- + \sigma_i^+)V(\mathbf{r}) = 2V_0(\mathbf{r}) - \frac{1}{2\pi} \sum_{i=1}^m (\sigma_i^- - \sigma_i^+) \int_{S_i} V(\mathbf{r}') \frac{\mathbf{r} - \mathbf{r}'}{|\mathbf{r} - \mathbf{r}'|^3} \cdot \mathbf{n} dS_i(r'). \quad (4.1)$$

Here S_i represents the surface of the respective conductivity interface within the volume conductor. σ_i^- and σ_i^+ represent the conductivities inside and outside the conductivity interface S_i respectively. $V_0(\mathbf{r})$ is the potential caused by the current source

in an infinite homogeneous medium given as,

$$V_0(\mathbf{r}) = \frac{1}{4\pi\sigma_0} \frac{\mathbf{q} \cdot \mathbf{R}}{R^3}, \quad (4.2)$$

where $\mathbf{R} = \mathbf{r} - \mathbf{r}'$, $R = |\mathbf{r} - \mathbf{r}'|$ and σ_0 is the unit conductivity (i.e., $\sigma_0 = 1$).

After calculating the potential, the magnetic field can be obtained using (Geselowitz, 1970)

$$\mathbf{B}(\mathbf{r}) = \mathbf{B}_0(\mathbf{r}) + \frac{\mu_0}{4\pi} \sum_{i=1}^m (\sigma_i^- - \sigma_i^+) \int_{S_i} V(\mathbf{r}') \frac{\mathbf{R}}{R^3} \times \mathbf{n} dS_i(r'), \quad (4.3)$$

with the unbounded magnetic field term \mathbf{B}_0 given by,

$$\mathbf{B}_0(\mathbf{r}) = \frac{\mu_0}{4\pi} \frac{\mathbf{q} \times \mathbf{R}}{R^3}. \quad (4.4)$$

To solve equation 4.1 numerically, the surface S_i is discretized into N area elements and surface integration can be obtained as a sum of the surface integrals on these elements:

$$\int_{S_i^j} \Delta\sigma_i^j V(\mathbf{r}') \frac{\mathbf{R}}{R^3} \cdot \mathbf{n} dS = \sum_{i=1}^N \int_{S_i^j} \Delta\sigma_i^j V(\mathbf{r}') \frac{\mathbf{R}}{R^3} \cdot \mathbf{n} dS, \quad (4.5)$$

where S_i^j represents the surface area of the j^{th} element on i^{th} surface. On each element, V is represented by a number of interpolation functions.

Using isoparametric elements enables us to express both the global coordinates and potentials on an element, using the same shape (interpolation) functions N_i , $i = 1 \dots m$, defined on the local coordinates (ξ, η, ν) of a parent element. That is,

$$x = \sum_{i=1}^m N_i(\xi, \eta, \nu) x_i^e \quad (4.6)$$

$$y = \sum_{i=1}^m N_i(\xi, \eta, \nu) y_i^e \quad (4.7)$$

$$z = \sum_{i=1}^m N_i(\xi, \eta, \nu) z_i^e \quad (4.8)$$

$$V = \sum_{i=1}^m N_i(\xi, \eta, \nu) V_i^e \quad (4.9)$$

where m is the number of nodes in an element, x_i^e , y_i^e , z_i^e are the coordinates and V_i^e is the potential of the i^{th} node. Since the parent element is planar, ν is a dependent variable (i.e., $\nu = 1 - \xi - \eta$). The elements could have linear ($m = 3$), quadratic ($m = 6$) or cubic ($m = 10$) approximation. The open form of the interpolation functions is provided in P2.

Let us express the surface integration on each element using the local coordinates (ξ, η) . Thus for the surface integral, we obtain

$$\int_S \Delta\sigma V(\mathbf{r}') \frac{\mathbf{R}}{R^3} \cdot \mathbf{n} dS' = \sum_{i=1}^N \int_0^1 \int_0^{1-\eta} \Delta\sigma V(\mathbf{r}') \frac{\mathbf{R}}{R^3} \cdot \mathbf{n} G d\xi d\eta, \quad (4.10)$$

where G is defined as,

$$G = \left| \frac{\partial \mathbf{r}}{\partial \xi} \times \frac{\partial \mathbf{r}}{\partial \eta} \right|. \quad (4.11)$$

The integral on the local coordinates can be approximated by using the Gauss-Legendre quadrature, which imposes to evaluate the integrand at n Gauss points, while multiplying each value with certain weights. That is, if f is the integrand, then

$$\int_0^1 \int_0^{1-\eta} f(\xi, \eta) d\xi d\eta \approx \frac{1}{2} \sum_{j=1}^n f(\xi_j, \eta_j) w_j. \quad (4.12)$$

The integration on the surface can be expressed as

$$\int_S \Delta\sigma V(\mathbf{r}') \frac{\mathbf{R}}{R^3} \cdot \mathbf{n} dS' = \sum_{i=1}^N \frac{1}{2} \sum_{j=1}^n \Delta\sigma V(\xi_j, \eta_j) w_j \frac{\mathbf{R}(\xi_j, \eta_j)}{R(\xi_j, \eta_j)^3} \cdot \mathbf{n}(\xi_j, \eta_j) g(\xi_j, \eta_j). \quad (4.13)$$

Since V at any local coordinate can be expressed in terms of node potentials, this integration can be written as

$$\int_S \Delta\sigma V(\mathbf{r}') \frac{\mathbf{R}}{R^3} \cdot \mathbf{n} dS' = \sum_{j=1}^M c_j V_j. \quad (4.14)$$

where c_j represents the contribution of the j^{th} node on the integration, and M is the total number of nodes on the surface. If V is to be calculated at M nodes, in matrix notation, we obtain

$$\mathbf{V} = \mathbf{A}\mathbf{V} + \mathbf{V}_0. \quad (4.15)$$

where \mathbf{V} is a column vector of potentials, \mathbf{A} is a square matrix whose elements are determined by the geometry and electrical conductivities of the regions of the model. \mathbf{V}_0 is the column vector of the potentials produced on the elements by the source alone, in an infinite medium. Once the coefficient matrix \mathbf{A} is calculated, the solution to \mathbf{V} can be obtained by

$$\mathbf{V} = [\mathbf{I} - \mathbf{A}]^{-1} \mathbf{V}_0, \quad (4.16)$$

where \mathbf{I} is an $M \times M$ identity matrix. Thus, by changing the dipole source location and strength (i.e., by changing the vector \mathbf{V}_0), a new solution can be obtained without affecting the \mathbf{A} matrix, which embodies the conductivity and structure information.

Deflating the A Matrix

At the outer boundary of the volume conductor we have Neumann boundary conditions. The partial derivative of the potential normal to the boundary is zero so the solution is unique up to an additive constant, i.e., the matrix $(\mathbf{I} - \mathbf{A})$ is singular. One solution to this problem is to use deflation method (Barnard et al., 1967; Lynn and Timlake, 1968; Hämäläinen and Sarvas, 1989). In this method, the matrix \mathbf{A} is replaced with the deflated version \mathbf{A}_d ,

$$\mathbf{A}_d = \mathbf{A} - \frac{1}{N} \mathbf{e}\mathbf{e}^T \quad \text{with} \quad \mathbf{A}\mathbf{e} = 0, \quad (4.17)$$

where \mathbf{e} is an $N \times 1$ vector with all entries equal to 1 and T represents the transpose operator. In our calculations we have employed a single deflation, since this is enough to eliminate the singularity in the \mathbf{A} matrix. Use of multiple deflations is known to reduce the number of iterations in the solution process (Hämäläinen and Sarvas, 1989).

4.2 Galerkin BEM with singularity extraction (P4)

In P4, the Galerkin method with high order basis functions is used to solve the forward problem. This method was previously used in the literature with linear elements and was called the triangle mean method (Lynn and Timlake, 1968). The piecewise linear basis functions with the Galerkin method are also reported (Mosher et al., 1999; Tissari and Rahola, 2003).

The potential V and magnetic field for a homogeneous conductor is calculated by solving

$$(\sigma^- + \sigma^+)V(\mathbf{r}) = 2V_0(\mathbf{r}) - \frac{(\sigma^- - \sigma^+)}{2\pi} \int_S \frac{\partial}{\partial n(\mathbf{r}')} \frac{1}{R} V(\mathbf{r}') dS(\mathbf{r}'). \quad (4.18)$$

Here S represents the surface of the volume conductor, σ^- and σ^+ respectively represent the conductivities inside and outside the sphere, $\mathbf{R} = |\mathbf{r} - \mathbf{r}'|$ and $\mathbf{r} \in S$. $V_0(\mathbf{r})$ represents the infinite medium potential given in equation 4.2.

After calculating the potential, the magnetic field can be calculated as

$$\mathbf{B}(\mathbf{r}) = \mathbf{B}_0(\mathbf{r}) + \frac{\mu_0}{4\pi} \sigma \int_S \nabla_{\mathbf{r}'} \left(\frac{1}{R} \right) \times \mathbf{n}(\mathbf{r}') V(\mathbf{r}') dS(\mathbf{r}') \quad (4.19)$$

assuming that \mathbf{r} is not located on S . The required primary magnetic field is given in equation 4.4.

The surfaces are triangulated with planar elements and the unknown potential is approximated with a linear combination of polynomial basis functions u_n ;

$$v^h(\mathbf{r}) = \sum_{n=1}^N \mathbf{c}_n u_n(\mathbf{r}). \quad (4.20)$$

Substituting this representation in equation 4.18, multiply it with test functions u_m , $m = 1, \dots, N$ and integrating over the surface results in matrix equation

$$\mathbf{A}\mathbf{c} = \mathbf{f}. \quad (4.21)$$

Here $\mathbf{c} = [c_1, \dots, c_N]^T$ is the unknown coefficient vector and the elements of \mathbf{A} and \mathbf{f} are given by

$$\begin{aligned} \mathbf{A}_{mn} &= \int_S u_m(\mathbf{r}) ((\sigma^- + \sigma^+) u_n(\mathbf{r})) \\ &+ \frac{1}{2\pi} (\sigma^- - \sigma^+) \int_S \frac{\partial}{\partial n(\mathbf{r}')} \left(\frac{1}{R} \right) u_n(\mathbf{r}') dS(\mathbf{r}') dS(\mathbf{r}) \end{aligned} \quad (4.22)$$

and

$$\mathbf{f}_m = 2 \int_S u_m(\mathbf{r}) g(\mathbf{r}) dS(\mathbf{r}). \quad (4.23)$$

Singularity extraction

Standard integration techniques such as Gaussian quadrature usually require the integrand to be sufficiently smooth. However, the integral kernel in equation 4.1 has a singular behavior of order $1/R$; where $R = |\mathbf{r} - \mathbf{r}'|$ is the distance between source point \mathbf{r}' and field point \mathbf{r} . The elements of the system matrix in equation 4.22 are assembled by evaluating the integrals between two triangles T_1 and T_2 at a time. When triangles T_2 and T_1 are close to each other (so called near singular case), the accurate evaluation of the term,

$$\int_{T_1} N_m^{(q)}(\mathbf{r}) \int_{T_2} \frac{\partial}{\partial n(\mathbf{r}')} \frac{1}{R} N_n^{(q)}(\mathbf{r}) dS(\mathbf{r}') dS(\mathbf{r}), \quad (4.24)$$

becomes difficult. Here $N_n^{(q)}$ is q^{th} order polynomial nodal shape function on triangle T_2 and $N_m^{(q)}$ on T_1 respectively. In order to solve the integral equation without sacrificing the accuracy of the solution, singularity extraction technique is used to compute the integrals (Järvenpää et al., 2003). The idea in this technique is to extract the singularity from the integrand of the inner integral in equation 4.24 and evaluate the extracted term in closed form. After the technique is applied, the implementation of the numerical integration becomes simpler since the remaining function is sufficiently smooth (Järvenpää et al., 2003).

The potential to be found in equation 4.18 is defined up to an additive constant (Hämäläinen and Sarvas, 1989). In order to provide a unique solution to the matrix equation, the deflation technique (Barnard et al., 1967) can again be applied as shown in equation 4.17.

4.3 FEM with Whitney Elements (P5)

If detailed nonhomogeneous and anisotropic conductivity information is available, e.g. from techniques such as diffusion tensor imaging (DTI) (Tuch et al., 2001) or magnetic resonance electrical impedance tomography (MREIT) (Seo et al., 2004), computation of the currents throughout the volume conductor is required (Yan et al., 1991; Thevenet et al., 1991; van den Broek et al., 1996; Awada et al., 1997; Haueisen et al., 1997; Wolters, 2003).

In the FEM, the 3D problem domain is partitioned into small volume elements, where particular properties can be assigned for each element. The elements can have various shapes such as tetrahedrons (P5) or cubes (P1, P3).

The corresponding weak formulation of the problem given equation 3.14 is: find such $u \in H^1(\Omega)$ that,

$$-\int_{\Omega} \nabla v \cdot \sigma \nabla u d\Omega(x) = \int_{\Omega} v \nabla \cdot \mathbf{J}_p d\Omega(x) \quad \forall v \in H^1(\Omega), \quad (4.25)$$

where v is the test function and $H^1(\Omega)$ stands for the standard Sobolev space of square integrable functions, whose first weak derivatives are also square integrable in Ω .

Dipole sources introduce singularity

The primary current sources are conventionally described by discrete current dipoles, which are implemented as singular point sources. This type of representation has the

advantage that being localized to a single point, it represents focal brain activity. Also, the calculation of lead fields corresponding to current dipoles is straightforward. However, point dipole sources introduce singularity into the integration. The FEM solution is based on a weak formulation of the conductivity equation and in order to be convergent, a certain degree of regularity is required from the source term. Singular sources such as point dipoles fail to satisfy the regularity requirement. As a consequence, the calculated fields depend on the location of the dipoles with respect to the finite element mesh (Awada et al., 1997). A method of treating the singularities that has been proposed in the literature is to subtract the analytically computed field of a dipole in homogeneous space from the total potential (Bertrand et al., 1991; van den Broek et al., 1996; Awada et al., 1997). However, these methods still lead to singular integrals that are difficult to evaluate numerically.

Whitney elements as sources

Alternatively, it is desirable to find a regular representation for localized current sources that allows directly the use of the standard weak form in FEM. Due to the vector source term, it is natural to represent the source current using *Whitney elements*. They have been successfully implemented in computational electromagnetics (Bossavit, 1998).

In (P5) we try to answer the following questions:

1. How do the fields generated by Whitney element sources compare to the fields generated by singular point sources?
2. Can we find a well-localized Whitney element source that produces approximately the same electromagnetic field as a singular current dipole?

Our purpose is to demonstrate that the Whitney element basis is capable of describing local activity, thus providing a reasonable and computationally flexible alternative for computing bioelectromagnetic fields in inhomogeneous and anisotropic media.

Whitney forms are a family of differential forms on a simplicial mesh (i.e. a network of tetrahedra, see figure 5.2(b)) as used in FEM. They are at most first degree polynomials on tetrahedra (Bossavit, 1988). The Whitney forms provide a hierarchy of basis functions that can be used to represent the qualitatively different electromagnetic quantities. The 0-forms represent scalar quantities such as electric potentials; the 1-forms represent field quantities such as electric and magnetic fields; the 2-forms represent flux quantities such as magnetic flux densities and current densities; the 3-forms represent volume quantities such as charge densities. The remarkable property of the Whitney forms is that the physically relevant continuity conditions across element boundaries are automatically satisfied and need not be imposed by extra conditions. Here we are interested only in the current densities, so the Whitney 2-forms are a natural choice for basis functions.

Let us define $\lambda_i, \lambda_j, \lambda_k$ to be standard first order nodal basis functions, the 2-form Whitney shape function for face f of tetrahedron is given as:

$$\mathbf{w}_f^{ijk} = 2(\lambda_i \nabla \lambda_j \times \nabla \lambda_k + \lambda_j \nabla \lambda_k \times \nabla \lambda_i + \lambda_k \nabla \lambda_i \times \nabla \lambda_j). \quad (4.26)$$

The basis functions $\mathbf{w}_j, j = 1 \dots F$ are defined for two tetrahedra adjacent to each other and vary linearly inside the volume of both tetrahedra between a vertex and the opposing face. Outside the two tetrahedra, the basis function vanishes. This type of basis function enables to model the current density on tetrahedra. Figure 4.2 depicts a

Whitney shape function in one of the two tetrahedra. The degrees of freedom are fluxes across the faces of the elements as opposed to nodes. The basis function guarantees that the normal component of current density is continuous across a face. Physically, the element can be thought to be as a H^1 -representation of a unit current dipole perpendicular to the ijk -face.

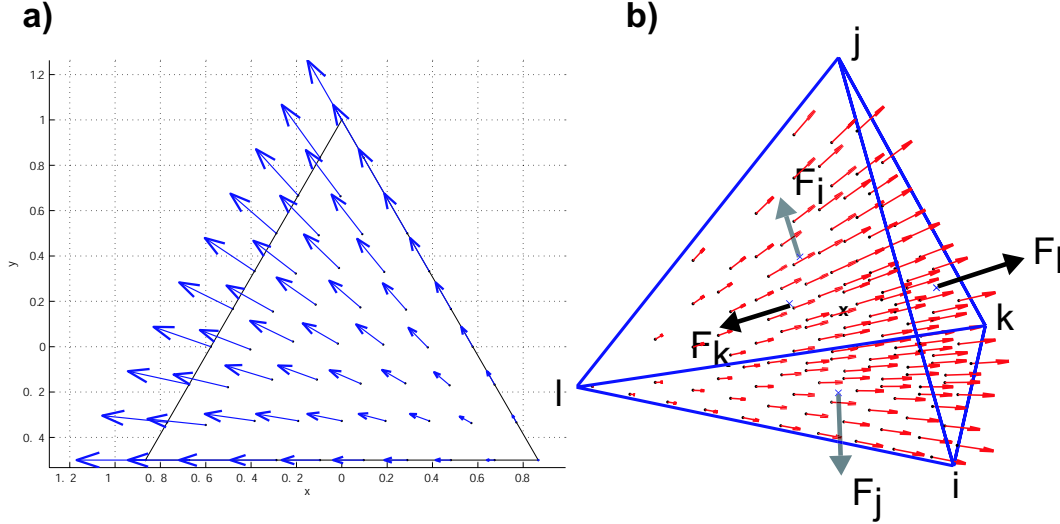


Figure 4.2: a) The visualization of the 2-form Whitney shape function on a flat triangle. b) The 2-form Whitney shape function for a tetrahedron. The shape function is evaluated for the face F_l opposing the vertex l of a tetrahedron. The basis function is defined such that the normal component of current density is continuous across the faces of the elements.

4.3.1 Calculation of the electric potential

Having defined the basis for the source current, we formulate the weak form for approximating numerically the electric potential.

Let u^h be a solution of the discretized problem

$$-\int_{\Omega} \nabla v^h(x) \cdot \sigma(x) \nabla u^h(x) d\Omega(x) = \int_{\Omega} v^h(x) \nabla \cdot \mathbf{J}_p^h(x) d\Omega(x). \quad (4.27)$$

The current inside an element can be approximated by facet elements, which are 2-form Whitney basis functions \mathbf{w}_j as

$$\mathbf{J}_p^h(x) = \sum_{j=1}^F c_j^h \mathbf{w}_j(x), \quad c_j^h \in \mathbb{R}, \quad (4.28)$$

coefficient c^h is the surface integral over a face and F is the number of interior faces in the mesh.

The scalar potential and the test functions are expressed with as

$$u^h(x) = \sum_{i=1}^N u_i^h \varphi_i(x), \quad u_i^h \in \mathbb{R} \quad (4.29)$$

and

$$v^h(x) = \sum_{i=1}^N v_i^h \varphi_i(x), \quad v_i^h \in \mathbb{R}, \quad (4.30)$$

where N is the number of nodes in the mesh. In this work, the functions φ_i are second order nodal polynomial basis functions on each element and are continuous across the element boundaries.

Let us denote

$$\mathbf{c}^h = [c_1^h, \dots, c_F^h]^T, \quad \mathbf{u}^h = [u_1^h, \dots, u_N^h]^T, \quad \mathbf{v}^h = [v_1^h, \dots, v_N^h]^T.$$

Now equation (4.27) can be written in matrix form as

$$(\mathbf{v}^h)^T \mathbf{A} \mathbf{u}^h = (\mathbf{v}^h)^T \mathbf{F} \mathbf{c}^h \quad \forall \mathbf{v}^h, \quad (4.31)$$

where

$$\mathbf{A}_{i,j} = - \int_{\Omega} \nabla \varphi_i(x) \cdot \sigma(x) \nabla \varphi_j(x) d\Omega(x), \quad 1 \leq i, j \leq N$$

and

$$\mathbf{F}_{i,j} = \int_{\Omega} \varphi_i(x) \nabla \cdot \mathbf{w}_j(x) d\Omega(x), \quad 1 \leq i \leq N, 1 \leq j \leq F.$$

Observe that the electric potential is unique up to an additive constant, and this fact has the consequence that the matrix \mathbf{A} has a one-dimensional null space. To make the solution of equation (4.27) unique, we fix the value of potential to zero in the first node of the mesh. This can be accomplished by zeroing the first row and column of matrix \mathbf{A} and then setting $\mathbf{A}_{1,1} = 1$. Further, we must zero the first row of the matrix \mathbf{F} . The discretized potential \mathbf{u}^h is then obtained as the solution of the system

$$\mathbf{A} \mathbf{u}^h = \mathbf{F} \mathbf{c}^h. \quad (4.32)$$

4.3.2 Calculation of the magnetic field

The current source term \mathbf{J} is considered to be consisting of \mathbf{J}_p , the primary current source and \mathbf{J}_s the secondary current source term due to volume effects. After scalar potential u is obtained, the magnetic field due to \mathbf{J} for a point sensor at location \mathbf{r}_i with orientation α_i can be calculated using

$$\begin{aligned} \alpha_i \cdot \mathbf{B}(\mathbf{r}_i) &= \frac{\mu_0}{4\pi} \int_{\Omega} (\mathbf{J}_p - \sigma \nabla u) \times \frac{\mathbf{r}_i - \mathbf{r}'}{|\mathbf{r}_i - \mathbf{r}'|^3} \cdot \alpha_i d\Omega(\mathbf{r}') \\ &= \frac{\mu_0}{4\pi} \int_{\Omega} (\mathbf{J}_p \times \frac{\mathbf{r}_i - \mathbf{r}'}{|\mathbf{r}_i - \mathbf{r}'|^3}) \cdot \alpha_i d\Omega(\mathbf{r}') \\ &\quad - \frac{\mu_0}{4\pi} \int_{\Omega} ((\sigma \nabla u) \times \frac{\mathbf{r}_i - \mathbf{r}'}{|\mathbf{r}_i - \mathbf{r}'|^3}) \cdot \alpha_i d\Omega(\mathbf{r}'). \end{aligned} \quad (4.33)$$

Let us define $\mathbf{B}^p \in \mathbb{R}^{M \times F}$ and $\mathbf{B}^s \in \mathbb{R}^{M \times N}$, where the matrix entries are given by

$$\mathbf{B}_{i,j}^p = \frac{\mu_0}{4\pi} \int_{\Omega} (\mathbf{w}_j \times \frac{\mathbf{r}_i - \mathbf{r}'}{|\mathbf{r}_i - \mathbf{r}'|^3}) \cdot \alpha_i d\Omega(\mathbf{r}'), \quad (4.34)$$

and

$$\mathbf{B}_{i,j}^s = - \frac{\mu_0}{4\pi} \int_{\Omega} (\sigma \nabla \varphi_j \times \frac{\mathbf{r}_i - \mathbf{r}'}{|\mathbf{r}_i - \mathbf{r}'|^3}) \cdot \alpha_i d\Omega(\mathbf{r}'). \quad (4.35)$$

In the previous expression, N , F , M denote the number of nodes, the number of source faces and the number of measurement points respectively. The approximation for the total magnetic field can be written as

$$\alpha_i \cdot \mathbf{B}(\mathbf{r}_i) = \mathbf{B}_{i,\cdot}^s \mathbf{u}^h + \mathbf{B}_{i,\cdot}^p \mathbf{c}^h. \quad (4.36)$$

Further using the presentation for \mathbf{u}^h from equation (4.32) in equation (4.36) we get

$$\mathbf{b}_{L \times 1}^h = \underbrace{(\mathbf{B}_{L \times N}^s \mathbf{A}_{N \times N}^{-1} \mathbf{F}_{N \times F} + \mathbf{B}_{L \times F}^p)}_{\mathbf{D}} \mathbf{c}_{F \times 1}^h. \quad (4.37)$$

We can then write a matrix equation for magnetic field as,

$$\mathbf{b} = \mathbf{D} \mathbf{c}^h. \quad (4.38)$$

The numerical implementation for the solution of equation (4.38) is explained in section 5.4.

Chapter 5

Numerical simulations

In this chapter, solutions of the forward problem obtained using the BEM and FEM formulations are presented. In the simulations described in this Thesis, the electric potential simulations on the outer surface points of the sphere are regarded as EEG measurements. The MEG measurements are simulated outside the sphere at locations simulating the magnetometers.

5.1 Error measure

The absolute error percentage is used in the comparison of potential in BEM simulations for single measurement points. The absolute error percentage is defined as

$$AE = 100 \cdot \frac{m_a - m_n}{m_a}, \quad (5.1)$$

where m_a is the potential value calculated using the closed form expressions for single or multi-layer spheres model and m_n is the value calculated numerically.

The relative difference measure (RDM) (Meijs and Peters, 1987) is used in the comparison of potential and magnetic field patterns using the closed form expressions for dipole sources. The percent RDM is defined as (Mosher et al., 1999)

$$RDM = 100 \cdot \sqrt{\frac{(\mathbf{v}_a - \mathbf{v}_n)^T (\mathbf{v}_a - \mathbf{v}_n)}{\mathbf{v}_a^T \mathbf{v}_a}}, \quad (5.2)$$

where \mathbf{v}_a is the vector of potential or magnetic field intensity values calculated using the analytical formulas and \mathbf{v}_n is the vector of potential or magnetic field intensity values calculated numerically.

5.2 BEM simulations of EEG with isoparametric elements (P1–P3)

In order to verify the validity of the new BEM formulation in P2, the numerical solutions must be compared with known analytical solutions, obtained for simple geometries. The head is usually modeled with a sphere, for which closed form expressions are readily available. The numerical results obtained for homogeneous and inhomogeneous sphere using the BEM are compared with the calculated analytical expressions presented in Chapter 3.

Because BEM integrations are performed only at the surface of the volume conductor, inner regions are not discretized as opposed to other numerical approaches,

like FEM or Finite Difference Method (FDM). To apply the BEM formulation, only the surface of the domain need to be discretized into small surface elements.

The new BEM formulation makes use of isoparametric elements, where quadratic and high order variations also allowed. We performed simulations for establishing the accuracy in the numerical solutions for a current dipole in homogenous sphere and the accuracy in the numerical solutions for a current dipole in inhomogeneous concentric spheres.

5.2.1 Homogeneous sphere model

Single layer, homogeneous sphere has been widely used in literature (Barnard et al., 1967; Brody et al., 1973; Cuffin, 1978; Budiman and Buchanan, 1993) for the calculation of the forward problem in electro-magnetic source imaging, because of the simplicity of the model. Using this model, forward calculations can be rapidly made since there are closed form expressions and an estimate for the solution of the inverse problem can be obtained. The performance of the new BEM formulation is verified using the closed form expression provided in section 3.4.1. A unit x-directed dipole in cartesian coordinates is located at (0,0,0.20) inside a homogeneous sphere with radius 1.

Table 5.1 shows error percentages attained with a mesh having 1026 nodes 2048 linear elements (column *Linear*) and a mesh with 512 quadratic elements (column *Quadratic*).

Table 5.1: Comparison of analytical and numerical solutions of potential for an x-directed dipole in cartesian coordinates located at (0,0,0.20) inside a single layer homogeneous sphere with radius 1. The comparison is done when the surface is discretized with 2048 linear elements and 512 quadratic elements.

x (unit)	y (unit)	z (unit)	Analytic (volt)	<i>Linear</i> BEM (volt)	<i>Quadratic</i> BEM (volt)	<i>Linear</i> Error %	<i>Quadratic</i> Error %
1.0	0.0	0.0	1.14	1.03	1.13	9.3219	1.19
0.91	0.0	0.40	1.29	1.18	1.28	8.444	0.58
0.82	0.0	0.57	1.28	1.17	1.27	8.044	0.37
0.70	0.0	0.70	1.20	1.11	1.20	7.820	0.29
0.57	0.0	0.82	1.05	0.97	1.04	7.789	0.34
0.40	0.0	0.91	0.81	0.74	0.80	7.931	0.52

The quadratic element type clearly outperforms the linear element, since the smooth geometry of the sphere is best represented with curved sided elements. Although, the homogeneous model is a simple and fast model for forward simulations, it is not realistic enough to model the head. Previous studies applying the homogeneous head model reported inaccurate localization results. Although some compensation schemes have been proposed (Kavanagh and Darcey, 1978; Ary et al., 1981; Salu et al., 1990; Berg and Scherg, 1994) to account for the smearing effect of the skull and other effects, a better model of the head must be used for an accurate forward and inverse problems.

5.2.2 Concentric shell model

Anatomically, the human head is composed of layers with differing conductivities. These layers are the brain, CSF, skull and scalp. For this simulation, a layered spherical mesh is used in order to have intrinsically homogeneous, but different conductivity regions. This type model is also called the multicompartment model of the head. The performance of the BEM formulation using the concentric shell model is verified using the closed form expressions provided in section 3.4.2.

A conductivity value of 0.005 S/m is assigned to the skull. The conductivity values for scalp and brain are taken nearly equal and are taken to be 0.2 S/m. Simulations are performed using a unit x -directed dipole in cartesian coordinates located at (0,0,0.15) inside a homogeneous sphere with unit radius.

Table 5.2: Comparison of analytical and numerical solutions of potential for an x -directed dipole in cartesian coordinates located at (0,0,0.15) inside a 3-layer concentric sphere model. The comparison is done when the surface is discretized with 2048 linear elements, 512 quadratic elements or 128 cubic elements.

x (unit)	y (unit)	z (unit)	Analytic (volt)	Linear BEM (volt)	Quadratic BEM (volt)	Cubic BEM (volt)	Linear Error %	Quadratic Error %	Cubic Error %
1.0	0.0	0.0	0.77	0.83	0.78	0.76	8.17	1.62	0.94
0.91	0.0	0.40	0.76	0.82	0.79	0.77	7.37	1.97	1.03
0.82	0.0	0.57	0.72	0.77	0.74	0.72	7.05	2.09	1.00
0.70	0.0	0.70	0.65	0.69	0.67	0.64	6.62	2.08	0.96
0.57	0.0	0.82	0.54	0.57	0.55	0.53	6.06	1.95	0.95
0.40	0.0	0.91	0.39	0.42	0.40	0.38	5.40	1.70	0.92

Table 5.2 shows the voltages and absolute error percentages for 2048 element-1026 node linear, 512 element-1026 node quadratic or 128 element-528 node cubic approximation mesh. The percentage error is best when cubic approximation is used followed by quadratic and linear approximation in BEM.

5.3 BEM simulations of EEG/MEG with singularity extraction technique (P4)

The forward problem solution for electric potential and magnetic field is calculated for the model configuration shown in Figure 5.2. To evaluate the numerical method, the closed formula for electric potential given in equation 3.30 and the formula for magnetic field given in equation 3.29 is used. The numerical calculation is based on the BEM formulation presented in section 4.2. The accuracy of the BEM solution using linear, quadratic and cubic approximation for the potential and magnetic field for a dipole is compared using RDM, as given in equation 5.2.

The result of the RDM comparison for the electric potential and magnetic field is shown in figure 5.1. The sphere mesh consists of 200, 794 and 1784 nodes for linear, quadratic and cubic approximations, respectively. Dipoles are placed on the

z-axis. In both figures, dashed lines represent the solutions obtained using only linear polynomial approximation keeping the node numbers same as in quadratic and cubic approximation on an element.

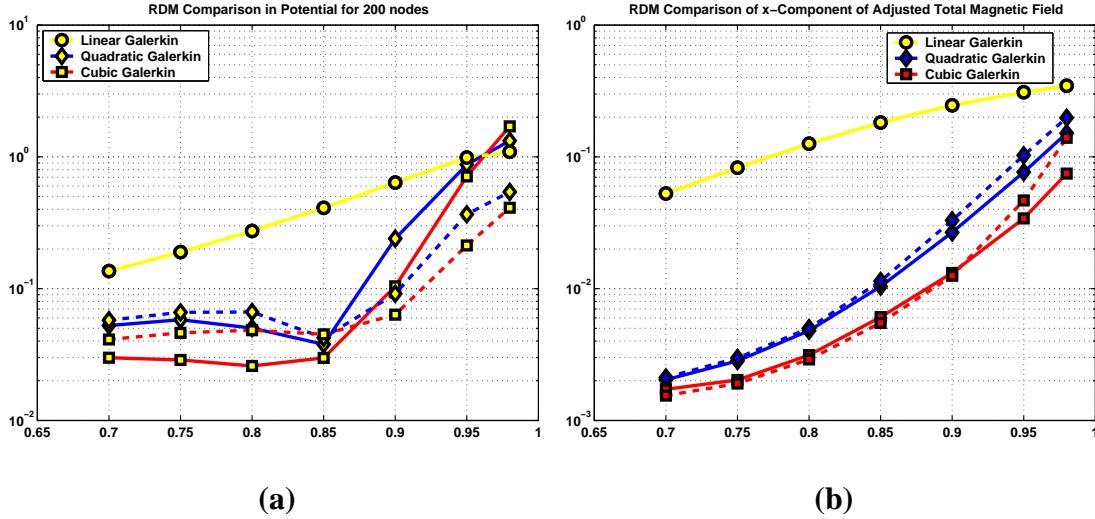


Figure 5.1: (a) The RDM in potential for nodes on the surface of the sphere. (b) The RDM in x-component of the magnetic field for a sensor cap consisting of 125 nodes. The mesh consists of 200, 794 and 1784 nodes for linear, quadratic and cubic approximations respectively. Dashed lines represent the solutions obtained using only linear polynomial approximation keeping the node numbers same as in quadratic and cubic approximation on an element. approximation.

5.4 FEM simulations of EEG and MEG with Whitney elements (P5,P6)

We are interested in finding out the correspondence between the voltage and magnetic fields calculated using the traditional singular current dipoles and the same values calculated using confined Whitney sources. This question is particularly relevant if one chooses to use the Whitney basis in MEG and EEG applications to localize brain activity. To compare the electric and magnetic fields, we choose spherical geometry since closed form expressions to calculate the magnetic field and potential for a current dipole are readily available (Sarvas, 1987; Zhang, 1995; Yao, 2000). The potential is calculated at point locations on a unit sphere and the magnetic field is calculated at point locations on a spherical cap, which is co-centered with the sphere on z-axis at 1.1 times the radius. The computation model is shown in figure 5.2(a).

For the purpose of FEM calculation, the sphere is divided into volume elements. A representative tetrahedral division of the sphere is shown in figure 5.2(b).

A general linear matrix equation relating the outside magnetic field to current density in terms of Whitney basis functions can be written as

$$\mathbf{b} = \mathbf{D}\mathbf{c}^h + \mathbf{e} \quad (5.3)$$

where \mathbf{e} is the possible measurement noise in the magnetic field, and \mathbf{D} is defined in equation (4.37).

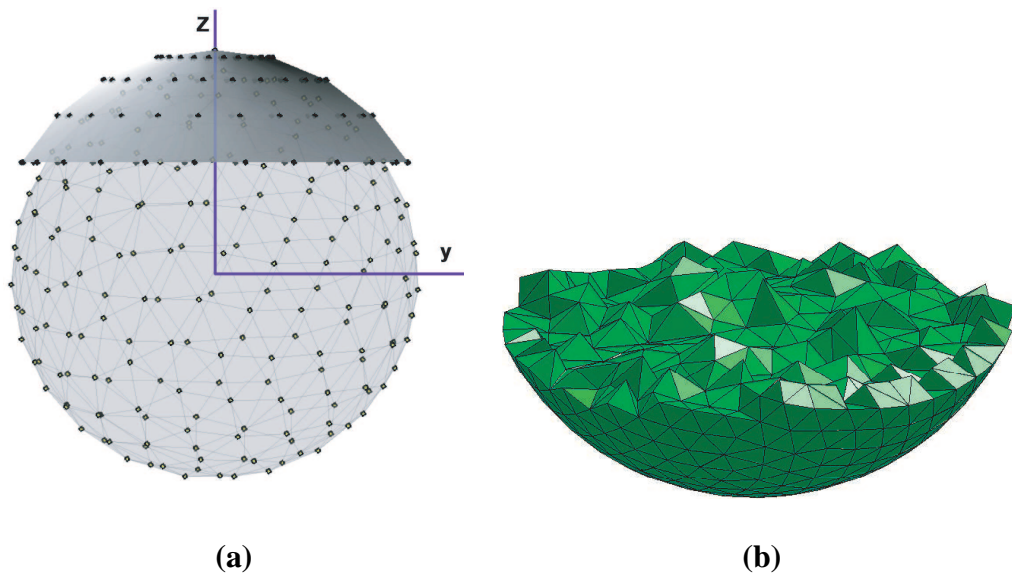


Figure 5.2: (a) Unit sphere model for the calculations. The electric field is calculated at points on the sphere. Magnetic field is calculated at the points on a cap located 1.1 times radius away from the sphere center. (b) Tetrahedral division of the sphere volume for FEM calculation. This is a linear mesh, 4 nodes per tetrahedron, has a total of 14804 elements-tetrahedrons, 2945 nodes and 28710 faces. There are 900 nodes and 1796 faces on the surface of the sphere.

The goal is to estimate the coefficient vector c^h based on the simulated measurements of b that are calculated here by using a singular dipole as a source in an arbitrary location. This is an *ill-posed problem*, due to the fact that the number of observation points is much less than the number of source coefficients and that numerically, the matrix D is of ill-determined rank, i.e., some of its singular values are close to or below of the working precision.

To obtain a useful estimate for c^h , some kind of regularization is needed. The selection of the regularization method has a qualitative effect on the solution of the biomagnetic inverse problem. By using the truncated SVD regularization or Tikhonov regularization, the estimated current densities are typically spread over a large volume (Hämäläinen et al., 1993). A good spatial localization can be achieved by using, e.g., the minimum current estimate (Uutela et al., 1999).

5.4.1 Continuous source coefficients

We are interested in evaluating the ability of Whitney elements to represent a locally confined source such as a point dipole at a known location. Therefore, we only pick certain faces with an aim to reproduce a well localized field pattern as observed for magnetic field and electric potential. In this respect, first we select only one tetrahedron which incorporates 4 coefficients, i.e one coefficient per face. We choose the tetrahedron that contains the point source producing the simulated data.

To represent the locally confined source with Whitney elements, the task is to find the coefficients c_i^h , which describe a field with a minimum error produced by a dipole, i.e we are looking for some c^h that satisfies equation (5.3) in the least square sense.

The solution of this equation is given as

$$\mathbf{c}^h = ((\mathbf{D}_{\cdot,J})^T (\mathbf{D}_{\cdot,J}))^{-1} (\mathbf{D}_{\cdot,J})^T \mathbf{b} \quad (5.4)$$

Here J is a set $\{i_1, i_2, i_3, i_4\}$ or $\{i_1, \dots, i_{16}\}$, where i_j are the numbers of the corresponding faces of the chosen tetrahedron that we aim to represent our confined source. The vector \mathbf{b} consists of given components of the magnetic field at the observation points. Reducing the size of the biomagnetic inverse problem does not render it well-posed, and the solution \mathbf{c}^h may be sensitive to errors in \mathbf{b} .

Every tetrahedron in the volume mesh has 4 faces, each shared with a neighboring tetrahedron's face. The Whitney coefficient \mathbf{c}^h is composed of 16 coefficients each representing a face of the neighboring tetrahedron depicted in figure 5.3.

The equation (5.4) represents the least square solution for the coefficients that best fit the measured field produced by the FEM solver employing Whitney elements and the analytical solution for the magnetic field calculated using a dipole. In a similar fashion, the best fit is found for the electric potential.

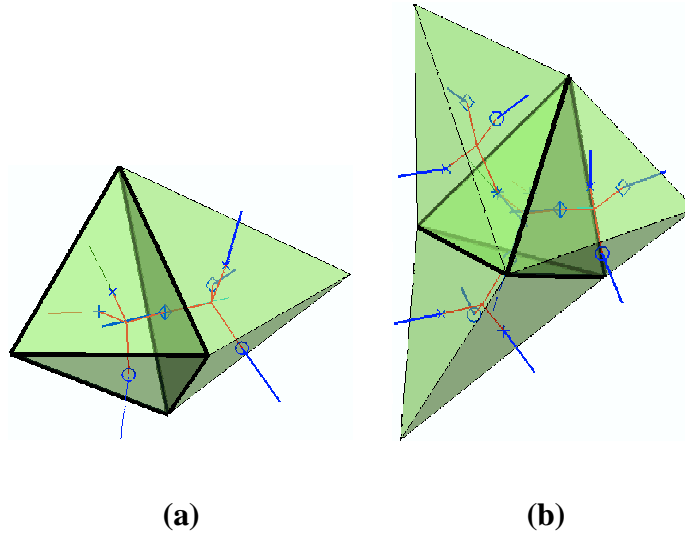


Figure 5.3: (a) Basic 2-form Whitney element configuration, a face representing one coefficient is shared by 2 tetrahedrons. (b) A Whitney source with 16 coefficients. The coefficients are all the faces of a common tetrahedron plus the four neighboring tetrahedrons sharing a face with the common tetrahedron.

For the analytical calculations, a single dipole source with moment $(1,0,0)$ is used. Sources are placed on z -axis with depths 0.20, 0.40, 0.60, 0.70, 0.80, 0.85, 0.89. Numerical calculations are carried out for 33 different FEM grids with varying element density to determine the convergence of the method. Grids consisting of uniform tetrahedra are generated from a surface triangulation, which serves as a seed for the volume grid generation. The seed surface triangulation itself is obtained from a uniform distribution of points on the sphere. The used mesh parameters are provided in Table 5.3. Figure 5.4 shows the obtained percent RDM results for potential and magnetic field, with source depth of 0.85 using all grids. In this example, 16 coefficients were fitted in the least squares sense to the dipole data. No artificial noise was added, i.e., the error term \mathbf{e} in equation 5.3 represent only the discrepancy between the dipole model and the Whitney element model. The trend of the convergence is obtained using a linear fit to the RDM values for the simulation. It is observed that, when a finer grid is

Table 5.3: Properties of some tetrahedral meshes used in the study.

Mesh No.	Seed Nodes	Nodes	Elements	Faces
1	1100	29,431	20,404	39,710
5	1500	45,663	31,982	62,466
10	2000	66,702	46,973	91,948
15	2500	88,571	62,680	122,862
20	3000	111,527	79,206	155,414
25	3500	136,110	96,947	190,396
30	4200	174,172	124,491	244,784
33	4800	205,757	147,366	289,934

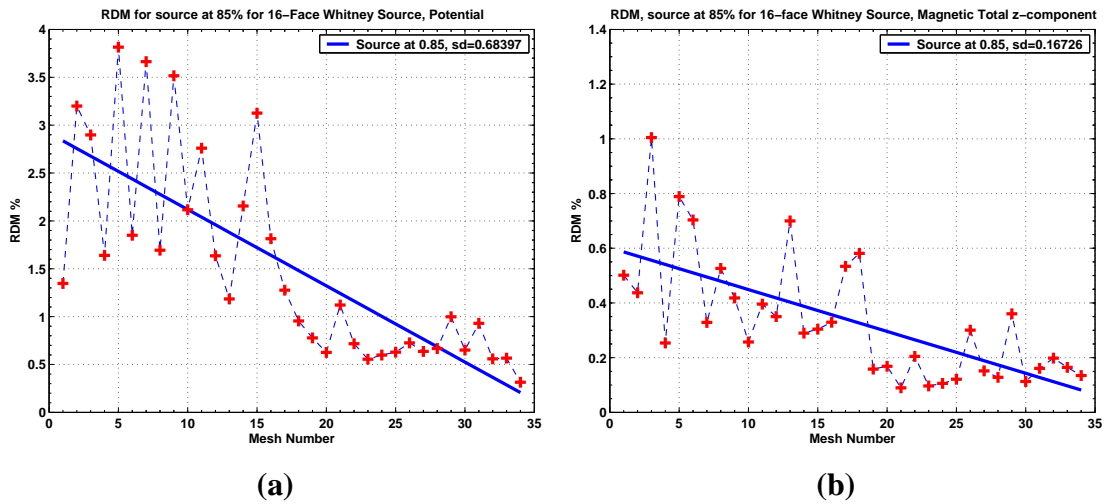


Figure 5.4: (a) The simulation results for potential, using 16-coefficients for a source centered at $(0,0,0.85)$. The figure depicts the change in percent RDM with various mesh sizes. (b) The simulation results for z-component of magnetic field in the same fashion. The straight line in both cases show the linear fit to the obtained RDM values with respect to different mesh sizes. Standard deviations from the linear fit are given in the figure legend.

used, the FEM formulation converges to the analytically calculated results. Figure 5.5 shows the RDM values for potential, which is calculated using different dipole depths. The y -component (tangential) of the magnetic field and the z -component (radial) of the magnetic field are presented in publication P5. It is observed that the percent RDM value increases when the dipole is close to the boundary of the spherical model. The Whitney-representation of the neuronal current calculated from the reference dipole is shown in figure 5.6. Figure 5.7 shows the volume of one tetrahedron in which the source is located at 0.80. Even though the mean volume of all tetrahedra in the grid decreases with increasing number of elements, the volume of the tetrahedron, inside which our source is located could be larger than the mean volume for that grid. This in turn affects the RDM result. However, for all source locations, the error reduced when grid size increased. Also, the source locations closer to the surface benefitted most from the increase in element density compared to sources at deeper locations.

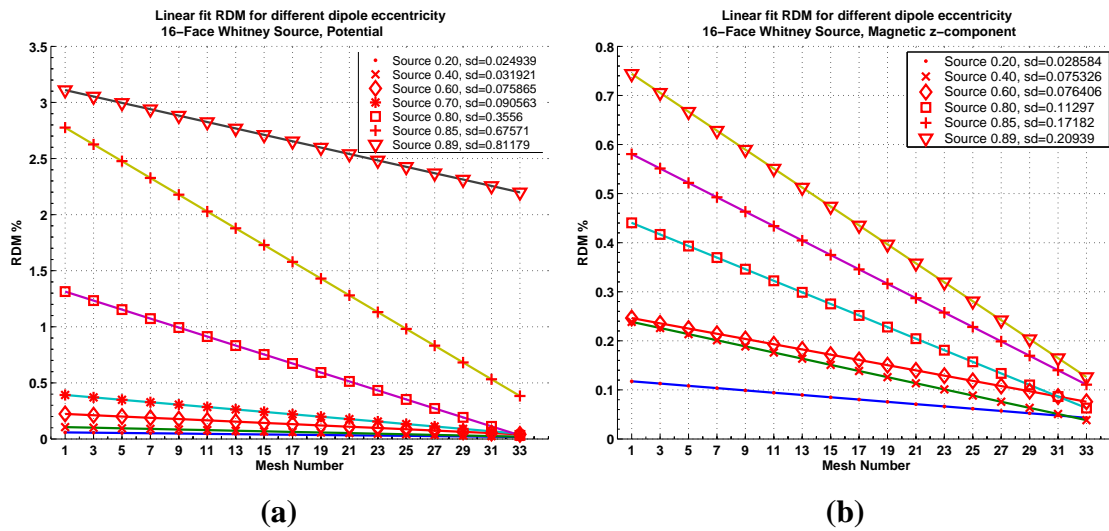


Figure 5.5: (a) RDM results for potential modeled by 16-coefficient source. (b) RDM results for z -component of magnetic field modeled by 16-coefficient source.

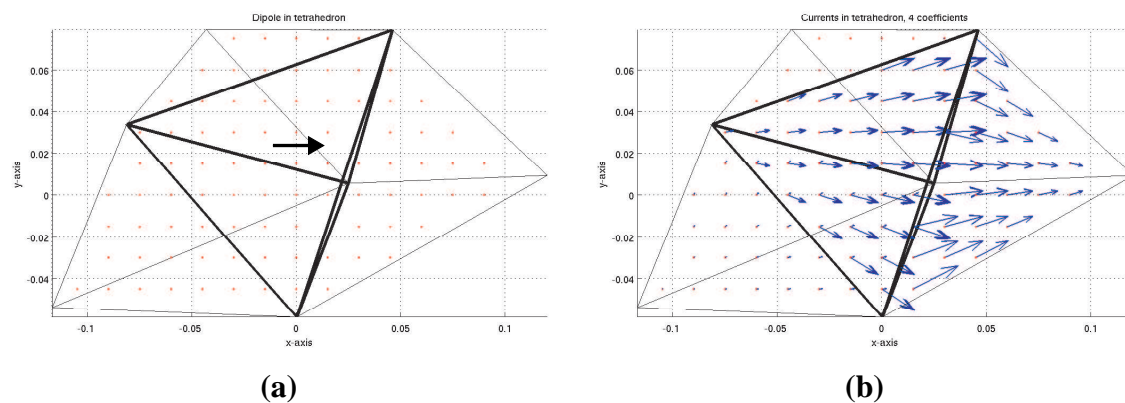


Figure 5.6: (a) A unit x -directed current dipole in cartesian coordinates inside tetrahedron. (b) Whitney representation of current dipole modeled using 4-coefficients.

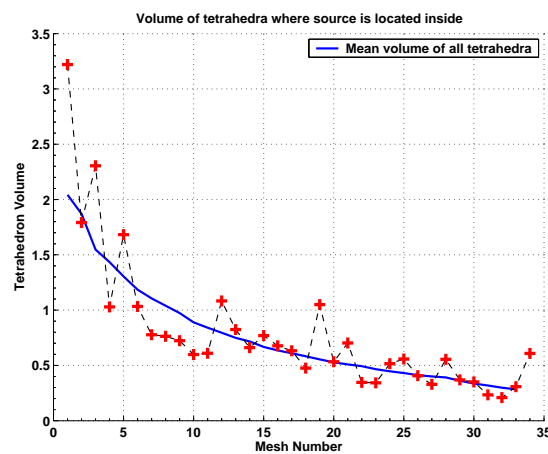


Figure 5.7: Individual points represent the volume of one tetrahedron where the source is located. Full line represents the mean volume of all tetrahedra for the same grid. The computations were done for a sphere with unit radius.

Chapter 6

Discussion

Bioelectromagnetic studies of the brain seeks to explore the properties of current generators, that are the sources of EEG and MEG measurements taking into account the nature of the head as a volume conductor of electricity. We can relate the measurements to physical properties, by developing mathematical models of the sources and the head. Starting from Maxwell's equations, expressions for magnetic field and electric potential have been derived.

It is agreed that, realistic models are the key elements in obtaining more accurate source distributions that represent the neural activity in the human brain. However, the geometry and conductivity structure of the problem becomes difficult with realistic models. Obtaining an analytical solution is not possible for volume conductors with complex geometry and conductivity structure. In this case, a numerical technique is needed to approximate the solution. The goal in this Thesis was to develop suitable numerical techniques with relatively high accuracy to solve the forward problem of bioelectromagnetic source localization. The BEM and FEM techniques were employed. Spherical geometry to test the accuracy of the numerical techniques was used, since fast and accurate analytical solutions are readily available. The performance of BEM and FEM are also compared with each other.

6.1 BEM studies, (P1– P4)

In publication P1 and publication P2, a new Boundary Element Method formulation, which uses isoparametric elements was presented. In publication P4, a Galerkin BEM formulation, which uses planar elements with high order basis functions was used. Singularity extraction technique (Järvenpää et al., 2003) is used to accurately evaluate near singular integrals. Software was prepared to solve the potential and magnetic field patterns for electric source imaging of the human brain. The appropriate boundary element mesh structures were formed using a mesh generation program that creates constant, linear, quadratic and cubic elements. A software was also prepared to calculate the EEG and MEG forward problem solution for single and multiple layer spheres.

Once the BEM coefficient matrix is built for the appropriate mesh structure, it is straightforward to solve for the field patterns for different dipole locations in the inverse problem. An iterative algorithm is used to solve the potential fields using the resultant matrix equation. For inverse problem solutions, the forward problem calculations must be repeated a number of times. Direct matrix inversion can be used to provide savings in computation time. However, this method requires a large amount of computer memory when the number of nodes is increased.

In publication P4, we investigated the performance of Galerkin approximation in

the calculation of forward problem solution. The results of the numerical accuracy are in agreement with previous studies using the Galerkin formulation for linear approximation of potential on each element (Mosher et al., 1999; Tissari and Rahola, 2003). Besides this, our work also included higher order basis functions, requiring six (quadratic) or ten (cubic) nodes per element. Also, the performance of higher order polynomial approximation on an element was compared to linear approximation when number of discretization nodes are kept the same. The results show that a more accurate potential approximation is needed when the sources are taken very close to the tessellated surface. Our opinion is that the quadratic and cubic potential approximations with Galerkin weighting is superior to linear approximation for deeper sources. However, for sources near the surface, more accurate representation of the model geometry is needed to achieve a lower error measure.

6.1.1 Factors affecting the performance of BEM, (P2)

If a realistically shaped head model is used, the accuracy in forward problem solutions can not be determined, since analytical expressions are not available for volume conductors of arbitrary shape. Instead, sphere model is used for testing the accuracy in numerical solutions. In general, as expected from a numerical method, the numerical accuracy is directly related to number of elements used in the discretization procedure and errors always decreased with increasing number of elements. Some factors effecting the accuracy of the calculations are discussed below.

Conductivity and thickness of the layers

Due to the low conductivity of the skull, an increase in the numerical errors have been observed. To overcome this problem, isolated problem approach (Hämäläinen and Sarvas, 1989; Meijs et al., 1989; Gençer and Akalin-Acar, 2005) has been implemented in the calculations, which reduced the overall relative errors in the model. The errors increase with a decreasing thickness between the layers. This is due to the numerical nature of the problem. Since, secondary sources are formed in the boundary layers, to catch the variation of the source, a better surface integration must be made. This is achieved by increasing the number of elements. Decrease of potentials in skull, depending on the thickness together with a smaller decrease through the scalp layer can be observed (Chauveau et al., 2004). Nevertheless, similar scalp potentials can be obtained using either a thick scalp layer and a thin skull layer. Thus, it is important to take into account the skull and scalp thicknesses, since the change in electric potential depends on both of these parameters.

Choice of Gauss points

In publication P2, evaluation of the surface integral in the discrete integral equation was done using Gauss Quadrature (Cowper, 1973). The integral function must be sampled very accurately in order to achieve satisfactory results, otherwise divergence is observed in the iteration process due to numerical noise. For the calculation of the numerical integration, we employed 7 point and 13 point integration rules for the quadratic element type, 6 point and 12 point rules for the cubic element type. We observed that the Gauss points should not be chosen close to element nodes since this can introduce further numerical contamination and divergence in the iteration process.

Dipole depth and local refinement

In a piecewise homogeneous volume conductor, the secondary sources are produced by the conductivity differences in the brain-skull and skull-scalp interfaces. For a deep dipole, small relative errors are observed. Although, some cortical structures are deep, most of the neural activity takes place in the cortex so shallow dipoles are assumed for accurate representation of the cortical activity. Changing the dipole location from center of the model to near the brain boundary causes absolute errors to be increased since the potentials near the dipole change fast. To overcome this error, either the total number of elements must be increased or local refinement of the model grid must be done, such as placing a larger number of elements to the upper hemisphere of the model. The latter is reasonable since EEG measurements are usually taken at small number locations where neural activity can take place and relatively low absolute errors are observed without increasing the total number of elements.

6.2 FEM studies

The FEM studies focus on accurate numerical simulation in bioelectromagnetic calculations with the purpose of improving inverse source modeling in the human head. For realistic simulations of the bioelectromagnetic forward problems, one should include all available and pertinent information of the object in the numerical model. Compared to BEM, FEM can easily handle inhomogeneity and anisotropy. The FEM formulation allows specifying physical properties such as a conductivity tensor for each element in the mesh. Thus, if available, realistic conductivity information of the head can be directly included in the computation of the forward problem. The price paid for this advantage is a need for high computational speed and computer resources.

6.2.1 FEM studies with Whitney elements, (P5, P6)

In publication P5, a new Finite Element Method formulation, which uses Whitney elements was derived and a software was prepared to solve the potential and magnetic field patterns for electric source imaging of the brain. The primary current is modelled using Whitney elements through face coefficients. The aim of the study, was to evaluate the performance of Whitney elements in representing a confined source such as a current dipole. A mesh generator software was used to construct the appropriate finite element mesh structure used in the calculations. The volume mesh composed of tetrahedral elements, that were generated from a given surface mesh, acting as seed. The seed surface mesh for the sphere model was created using another software that optimized an equidistant placement of nodes and triangles on the sphere. This was done to minimize mesh artifacts on the numerical accuracy.

The results in publication P5, show that, in the forward problem solution, Whitney element formulation behaves reasonably well with low percentage RDM errors for the chosen dipole eccentricity. This implies that Whitney elements are good alternatives to point dipole sources to represent neural currents.

In the following study, publication P6, the Whitney element formulation is extended to model both primary and secondary currents in terms of Whitney-type elements. Secondary currents can affect the forward problem results, especially if the conductivity properties of neural tissue exhibit strong anisotropy.

Continuous current sources

Biological currents are continuous in the neural tissue. The primary currents in MEG and EEG arise mainly in the cortex from postsynaptic intracellular currents which are represented with discrete current dipoles (Wikswow et al., 1980). The motivation to use Whitney form of finite elements is based on the ability of these elements to represent continuous nature of primary currents in the neural tissue. Instead of dipoles, sources are estimated to be confined to a small number of elements and current is modeled to be continuous through faces of the adjacent elements. With these properties, the Whitney element formulation enables us to avoid point singularities and numerical instability in the computations, thus providing accurate results.

Results using RDM measure

The RDM provides us an overall measure of differences in fields between numerical and analytical calculations for different source locations. In publication P5, using this measure, results are provided to evaluate the effect of source location, grid size and the size of Whitney element coefficient vector in the simulations. Generally, accuracy of the numerical method is related to the number of elements used in the discretization. It is expected that the numerical errors are lower with increasing number of elements, i.e. decreasing volumes of the elements. In our simulations we observed this behavior (publication P5). Sources, which are very near to the sphere surface gave worse RDM results compared to deeper ones due to steep field change (publication P5). Using more coefficients i.e., more elements adjacent to the point source location, provided better RDM values.

The oscillatory behavior in RDM results observed are attributed to the properties of the tetrahedral volume grid for which the simulation is performed, i.e., how the forward model dipole is located with respect to the FEM faces. The final quality of mesh depends on the positions of the nodes inside the sphere volume, which are automatically added by the mesh generator program during the generation process. As a result, the solutions we obtained depended especially on the quality of the tetrahedra around our source point, given the fact that, there was small difference in the number of surface seed nodes provided to the mesh generator program for generating the volume grids. Therefore, we attribute the volume of the tetrahedron to be a direct factor, affecting our results.

6.3 Comparison of BEM and FEM, (P1, P3)

BEM has relative merits compared to FEM when solving for the potential on the scalp and the magnetic field nearby the head. BEM, as the name implies, only requires a mesh at the boundaries of each region, which generates solutions only at the boundaries. On the other hand FEM requires discretization in the full domain of interest, thereby yielding large number of elements and nodes. Considering the physical structure of the head, we are able to model it as a piecewise homogeneous conductor. This enables BEM to be employed for this type of problem easily. Solutions of the potential and magnetic field can be calculated using BEM with fewer elements and satisfactory accuracy levels. The parallel implementation of the FEM provides a means for solving large size problems (Acar and Gençer, 2002; Wolters et al., 2002). As the performance of workstations and local area networks increase, using the computational equipment

in a small laboratory environment, a workstation cluster becomes an attractive platform for high performance computing (Acar and Gençer, 2002). With this kind of architecture, it is possible to solve field problems using FEM, that are too time consuming for a single workstation. However, to gain the maximum efficiency from parallel platforms the algorithms must be carefully selected, revised and tuned.

Performance comparison of BEM and FEM

The performance of the BEM formulation is evaluated for a single dipole source located at different points on the z-axis in a concentric sphere model. Three numerical models are developed using three isoparametric element types (elements that support linear, quadratic, or cubic variation). The number of nodes is kept approximately equal in different meshes. In publication P2, the percentage RDM value is calculated to be on the order of 7% for linear elements, and this is comparable to the RDM values previously found in the literature (Schlitt et al., 1995). The RDM for quadratic and cubic elements vary between 1.2% and 1.7% when using BEM. It is observed that, in general, RDM is much smaller when the quadratic and cubic elements are used in the numerical model. For magnetic field solutions, first a homogeneous sphere is assumed to represent the inner region of the skull. The field points are assumed to be placed on a hypothetical sphere of radius 1.1 times the unit sphere radius. The RDM is on the order of 1% for the linear-element mesh, 0.03% for the quadratic-element mesh, and 0.01% for the cubic-element mesh. When the skull layer is added in the model, RDM in numerical solutions rise to a maximum of 0.07% when quadratic elements are used in the model. Potential solutions using FEM (Acar and Gençer, 1999), are also evaluated with concentric-sphere model used in the BEM studies. With a similar source configuration, the RDM is found to be less than 0.3%. For magnetic field calculations, when the potential function is solved using FEM, the RDM is observed to be below 1.6%.

6.4 Effects of tissue conductivity anisotropy

The BEM assumes isotropic conductivities for the major tissue types. However, it is known that there is anisotropic behavior in tissue conductivity of the human head. With FEM, it is possible to include detailed conductivity information in the volume conductor properties and solve the forward problem with this incorporated information.

It was previously reported that conductivity anisotropy has a large effect on the scalp EEG distribution (Marin et al., 1998). Conductivity anisotropy is especially observed in the gray matter, fiber tracts of the white matter and the skull (Wolters, 2003). Anisotropic conductivity in white matter causes return currents to flow in directions parallel to the white matter fiber tracts. For deep sources, the effect of anisotropy on EEG and MEG increases with the amount of anisotropic tissue surrounding the source (Wolters et al., 2005). Also a large influence was observed on the amplitude of EEG and MEG due to conductivity anisotropy in the single dipole modeling case (Hauelsen et al., 1997, 2002). For EEG, the presence of anisotropy both for the skull and white matter tissue affects the potential computations in the forward problem hence, the inverse source reconstructions. In contrast, for the MEG, only the anisotropy of the white matter compartment has a significant effect.

The use of FEM provides robust way to evaluate the effect of anisotropy in the

forward and inverse modeling of EEG and MEG. Usually, the conductivity values used in the numerical models are average values based on various observations. In order to achieve realistic head models with ultimate accuracy, it is better to use individually measured conductivity values. However, non-invasive measurement of tissue electrical conductivity is itself a difficult problem to be solved.

6.5 Future developments

In general, both BEM and FEM formulations produce accurate potential and magnetic field solutions. All these numerical techniques, however, require state-of-the-art segmentation methods and mesh generation algorithms to develop realistic head models. If the extracted surfaces are not correct then the use of higher-order elements is questionable. Thus, in order to achieve better forward problem solutions, the segmentation algorithm should provide accurate geometrical information for every tissue type in the head. In addition to the errors regarding the geometry of different tissue types, the correct electrical conductivity model of the human head should also be employed to obtain a realistic head model.

Methods that are discussed in this Thesis are suitable also for finding electrical source distributions of the heart. The electrical (ECG) and magnetic measurements (MCG) can also be obtained from the torso surface and near the torso (Barnard et al., 1967; Geselowitz, 1967; Cohen and Chandler, 1969; Geselowitz, 1970). The thorax and heart geometry together with conductivity information can be employed to develop realistic torso models (Horacek, 1974; Barr et al., 1977; Gulrajani and Mailloux, 1983; van Oosterom and Huiskamp, 1991; Nenonen et al., 1991; MacLeod et al., 1991; Johnson et al., 1992; Zhou and van Oosterom, 1994; Bruder et al., 1994; Malmivuo and Plonsey, 1995; Pullan, 1996; Tenner et al., 1997; Ramon et al., 1998).

Chapter 7

Conclusions

This work describes improvements in methods for the forward problem solution of brain electromagnetic source imaging. The purpose of the studies is to pave the way for obtaining better localization of the brain generated electromagnetic sources. This can be achieved by improving the accuracy of the forward problem solution. Using better head models, we can obtain more accurate source descriptions that represent the neural activity in the human brain. Individual or average geometries of the head are better models than spheres to represent the head. Since analytical solutions are not available for realistic geometries, the use of numerical methods is essential.

The work presented in this Thesis strives to explore the performance of BEM and FEM in the forward problem solution. The numerical methods were compared against analytical solutions using a test model. The test model is a unit sphere with a single current dipole representing the neuronal activity within the sphere. The unit sphere model is ideal for testing numerical algorithms since exact solutions are easy and fast to compute. The BEM and FEM are also compared with each other for accuracy in the forward problem.

The publications included in the Thesis describe new ways of computing the forward problem in source localization: Publication P2 discusses a new BEM formulation with isoparametric elements. Using isoparametric elements enable better representation of the physical properties of the model. In publication P4 the performance of BEM with Galerkin weighting was studied for the forward problem solution. Singularity extraction technique is employed to tackle the problem of numerically evaluating near singular integrals. It is observed that the quadratic and cubic potential approximations with Galerkin weighting is superior to linear approximation for deeper sources. However, for sources near the surface, more accurate representation of the model geometry is needed to achieve a better error measure.

Publications P1 and P3 formulate and compare the numerical solutions obtained using the BEM and FEM. The numerical methods have their relative merits when solving for the potential on the scalp and the magnetic field outside the head. BEM, only requires a mesh at the boundaries of the volume conductor. This reduces the computational requirements for volume conductor modeling and numerical analysis where number of elements and nodes in the mesh are the determining factors. FEM on the other hand, requires discretization or meshing of the full domain of the volume conductor. Nodes and elements are generated within the volume of interest, as well as the boundary. This is computationally costly and yields large number of elements and nodes. Use of parallel computing resources is a way to overcome this problem.

Publications P5 and P6 introduce the Whitney elements. The current source can be represented as a continuous entity rather than a point dipole, which is widely used to represent current sources in the brain. In this respect, the Whitney element formulation

might serve a better model to represent primary currents in neural tissue. In addition, FEM formulation allows us to specify a conductivity tensor for each tetrahedral element in the mesh. Thus, if available, realistic conductivity information on the head can be directly included in the computation of the forward problem.

Although realistic head models promise more accurate localization results, the realistically shaped conductor model did not replace the spherical model in mainstream use. This is partly because of the difficulties in generating accurate individual computational models rapidly, due to lack of robust image processing techniques such as segmentation and three dimensional mesh generation. In addition the computational cost of the numerical methods such as BEM and FEM are still preventive for individual analysis. Another future challenge is obtaining and embedding of individual anisotropic conductivity information of the brain into the computational model. The FEM is the most suitable technique to be able to utilize this information with a drawback of increased computational cost, since the volume of the computation domain needs to be discretized. However, it is expected that more accurate EEG/MEG source localization will be possible with the advent of faster computers and new image acquisition-processing techniques. These developments would bring practicality to the process of creating better computational models based on individual anatomy and realistic physical properties.

Bibliography

- Acar, C. and Gençer, N. G. (1999). Forward problem solution of esi using fem and bem with quadratic isoparametric elements. In *Proceedings of the First Joint BMES-EMBS Conference*, Atlanta, GA, USA. BMES-EMBS, Omnipress.
- Acar, C. E. and Gençer, N. G. (2002). A high performance pc-based parallel computing platform for electro-magnetic source imaging. *Int. J. Bioelectromagnetism*, 4:217–218.
- Ahonen, A. I., Hämäläinen, M. S., Kajola, M. J., Knuutila, J. E. T., Laine, P. P., Lounasmaa, O. V., Parkkonen, L. T., Simola, J. T., and Tesche, C. D. (1993). A 122-channel SQUID instrument for investigating the magnetic signals from the human brain. *Physica Scripta*, T49:198–205.
- Ary, J. P., Klein, S. A., and Fender, D. H. (1981). Location of sources of evoked potentials: Corrections for skull and scalp thicknesses. *IEEE Trans. Biomed. Eng.*, 28:447–452.
- Awada, K., Jackson, D., Williams, J., Wilton, D., Baumann, S., and Papanicolau, A. (1997). Computational aspects of finite element modeling in EEG source localization. *IEEE Trans. Biomed. Eng.*, 44:736–752.
- Ayache, N. (1997). Medical image analysis and simulation. In *Asian Computing Science Conference*, pages 4–17.
- Barnard, A., Duck, I., Lynn, M., and Timlake, W. (1967). The application of electromagnetic theory to electrocardiography. II. Numerical solution of the integral equations. *Biophys. J.*, 7:433–462.
- Barr, R. C., Ramsey, M., and Spach, M. S. (1977). Relating epicardial to body surface potentials by means of transfer coefficients based on geometry measurements. *IEEE Trans. Biomed. Eng.*, 24:1–11.
- Belliveau, J. W., Kennedy, D. N., McKinstry, R. C., Buchbinder, B. R., Weisskopf, R. M., and Cohen, M. S. (1991). Functional mapping of the human visual cortex by magnetic resonance imaging. *Science*, 254:716–719.
- Berg, P. and Scherg, M. (1994). A fast method for forward computation of multiple-shell spherical head models. *Electroenceph. Clin. Neurophys.*, 90:58–64.
- Berger, H. (1929). Über das elektrenkephalogramm des menschen. (on the electroencephalogram in man). *Arch. Psychiatr. Nervenkr.*, 87:527–543.
- Bertrand, O., Thevenet, M., and Perrin, F. (1991). 3-d finite element method in brain electrical activity studies. Technical Report TTK-F-A689, HUT.

- Bezdek, J., Hall, L., and Clarke, L. (1993). Review of mr image segmentation techniques using pattern recognition. *Med. Phys.*, 20:1033–1048.
- Bossavit, A. (1988). Whitney forms: a class of finite elements for three-dimensional computations in electromagnetism. *IEEE Proc. A*, 135:493–500.
- Bossavit, A. (1998). *Computational electromagnetism*. Academic Press Inc., San Diego CA.
- Brody, D. A., Terry, F. H., and Ideker, R. E. (1973). Eccentric dipole in a spherical medium: Generalized expression for surface potentials. *IEEE Trans. Biomed. Eng.*, 20:141–143.
- Bruder, H., Killmann, R., Moshage, W., Weismuller, P., Achenbach, S., and Bommel, F. (1994). Biomagnetic localization of electrical current sources in the human heart with realistic volume conductors using the single-current-dipole model. *Physics in Medicine and Biology*, 39:655–668.
- Bruno, A. C. and Romani, G. L. (1989). Neuromagnetic localization performed by using planar gradiometer configurations. *J. Appl. Phys.*, 65:2098–2101.
- Budiman, J. and Buchanan, D. (1993). An alternative to the biomagnetic forward problem in a realistically shaped head model, the weighted vertices. *IEEE Trans. Biomed. Eng.*, 40:1048–1055.
- Chauveau, N., Franceries, X., Doyon, B., Rigaud, B., Morucci, J., and Celsis, P. (2004). Effects of skull thickness, anisotropy, and inhomogeneity on forward EEG/erp computations using a spherical three-dimensional resistor mesh model. *Hum. Brain. Mapp.*, 21:86–97.
- Chunlin, L., Goldgof, D. B., and Hall, L. O. (1993). Knowledge-based classification and tissue labeling of mr images of human brain. *IEEE Trans. Med. Imag.*, 12:740–750.
- Cohen, D. (1968). Magnetoencephalography, evidence of magnetic fields produced by alpha-rhythm currents. *Science*, 161:784–786.
- Cohen, D. (1972). Magnetoencephalography: Detection of the brain's electrical activity with a superconducting magnetometer. *Science*, 175:664–666.
- Cohen, D. and Chandler, L. (1969). Measurements and simplified interpretation of magnetocardiograms from humans. *Circulation*, 39:395–402.
- Cowper, G. R. (1973). Gaussian quadrature for triangles. *Int. J. Numer. Meth. Eng.*, 7:405–408.
- Cuffin, B. N. (1978). On the use of electric and magnetic data to determine sources. *Ann. Biomed. Eng.*, 6:173–193.
- Cuffin, B. N. (1990). Effects of head shape on EEG's and MEG's. *IEEE Trans. Biomed. Eng.*, 37:44–52.
- Cuffin, B. N. (1991). Eccentric spheres models of the head. *IEEE Trans. Biomed. Eng.*, 38:871–878.

- Cuffin, B. N. (1993). Effects of local variations in skull and scalp thickness on EEG's and MEG's. *IEEE Trans. Biomed. Eng.*, 40:42–48.
- Cuffin, B. N. (1996). EEG localization accuracy improvements using realistically shaped head models. *IEEE Trans. Biomed. Eng.*, 43:299–303.
- Cuffin, B. N. and Cohen, D. (1977). Magnetic fields of a dipole in special volume conductor shapes. *IEEE Trans. Biomed. Eng.*, 24:372–381.
- Cuffin, B. N., Yunokuchi, K., Maniewski, R., Purcell, C., Cosgrove, G. R., Ives, J. R., Kennedy, J., and Schomer, D. (1990). MEG versus EEG localization test using implanted sources in the human brain. *Ann. Neurol.*, 28:811–817.
- da Silva, F. L. and van Rotterdam, A. (1987). *Biophysical aspects of EEG and MEG generation*, pages 15–28. Urban and Schwarzenberg, Baltimore, 2 edition.
- Dawson, G. (1947). Cerebral responses to electrical stimulation of peripheral nerves in man. *J. Neurol. Neurosur. Ps.*, 10:137–140.
- de Munck, J. C. (1988). The potential distribution in a layered anisotropic spheroidal volume conductor. *J. Appl. Phys.*, 64:461–470.
- de Munck, J. C. (1993). A fast method to compute potential in the multisphere model. *IEEE Trans. Biomed. Eng.*, 40:1166–1174.
- Ding, L. and Y. Lai, B. H. (2005). Low resolution brain electromagnetic tomography in a realistic geometry head model: a simulation study. *Phys. Med. Biol.*, 50:45–56.
- Eshel, Y., Witman, S. L., Rosenfeld, M., and Abboud, S. (1995). Correlation between skull thickness and asymmetry and scalp potential estimated by a numerical model of the head. *IEEE Trans. Biomed. Eng.*, 42:242–259.
- Frank, E. (1952). Electric potential produced by two point current sources in a homogeneous conducting sphere. *J. Appl. Phys.*, 23:1225–1228.
- Fuchs, M., Kastner, J., Wagner, M., Hawes, S., and Ebersole, J. (2002). A standardized boundary element method volume conductor model. *Clin. Neurophysiol.*, 113:702–712.
- Fuchs, M., Wagner, M., and Kastner, J. (2001). Optimum boundary element method volume conductor models. In Nenonen, J., Ilmoniemi, R., and Katila, T., editors, *Proc. 12th Int. Conf. on Biomagnetism*, Espoo, Finland. Helsinki Univ. of Technology.
- Geisler, C. D. and Gerstein, G. L. (1961). The surface EEG in relation to its sources. *Electroenceph. Clin. Neurophys.*, 13:927–934.
- Gençer, N. G. and Akalin-Acar, Z. (2005). Use of the isolated problem approach for multi-compartment bem models of electro-magnetic source imaging. *Phys. Med. Biol.*, 50:3007–3022.
- Geselowitz, D. B. (1967). On bioelectric potentials in an inhomogeneous volume conductor. *Biophys. J.*, 7:1–11.

- Geselowitz, D. B. (1970). On the magnetic field generated outside an inhomogeneous volume conductor by internal current sources. *IEEE Trans. Magn.*, 6:346–347.
- Gulrajani, R. M. and Mailloux, G. E. (1983). A simulation study of the effects of torso inhomogeneities on electrocardiographic potentials using realistic heart and torso models. *Circ. Res.*, 52:45–56.
- Hall, L., Bensaid, A., Clarke, L., Velthuizen, R., Silbiger, M., and Bezdek, J. (1992). A comparison of neural networks and fuzzy clustering techniques in segmenting magnetic resonance images of the brain. *IEEE Trans. Neural Networks*, 3:672–682.
- Hämäläinen, M. S., Hari, R., Ilmoniemi, R. J., Knuutila, J., and Lounasmaa, O. V. (1993). Magnetoencephalography — theory, instrumentation, and applications to noninvasive studies of the working human brain. *Rev. Mod. Phys.*, 65:413–497.
- Hämäläinen, M. S. and Sarvas, J. (1989). Realistic conductivity geometry model of the human head for interpretation of neuromagnetic data. *IEEE Trans. Biomed. Eng.*, 36:165–171.
- Haralick, R. M. and Shapiro, L. G. (1985). Image segmentation techniques. *Computer Vision, Graphics, and Image Processing*, 29:100–132.
- Hari, R., Joutsiniemi, S. L., and Sarvas, J. (1988). Spatial resolution of neuromagnetic records: theoretical calculations in a spherical model. *Electroenceph. Clin. Neurophys.*, 71:64–72.
- Haueisen, J., Ramon, C., Eiselt, M., Brauer, H., and Nowak, H. (1997). Influence of tissue resistivities on neuromagnetic fields and electric potentials studied with a finite element model of the head. *IEEE Trans. Biomed. Eng.*, 44:727–735.
- Haueisen, J., Schack, B., Meier, T., Curio, G., and Okada, Y. (2001). Multiplicity in the high-frequency signals during the short-latency somatosensory evoked cortical activity in humans. *Clin. Neurophys.*, 112:1316–1325.
- Haueisen, J., Tuch, D., Ramon, C., Schimpf, P., Wedeen, V., George, J., and Belliveau, J. W. (2002). The influence of brain tissue anisotropy on human EEG and MEG. *Neuroimage*, 15:159–166.
- He, B., Musha, T., Okamoto, Y., Homma, S., Nakajima, Y., and Sato, T. (1987). Electric dipole tracing in the brain by means of the boundary element method and its accuracy. *IEEE Trans. Biomed. Eng.*, 34:406–414.
- Helmholtz, H. (1853). Ueber einige Gesetze der Vertheilung elektrischer Ströme in körperlichen Leitern, mit Anwendung auf die thierisch-elektrischen Versuche. *Ann. Phys. Chem.*, 89:211–233, 353–377.
- Horacek, B. (1974). Numerical model of an inhomogeneous human torso. In Rush, S. and Lepeshkin, E., editors, *Advances in Cardiology*, volume 10, pages 51–57. S. Karger, Basel.
- Janday, B. S. and Swithenby, S. J. (1987). Analysis of magnetoencephalographic data using the homogeneous sphere model: empirical tests. *Physics in Medicine and Biology*, 32:105–113.

- Järvenpää, S., Taskinen, M., and Ylä-Oijala, P. (2003). Singularity extraction technique for integral equation methods with higher order basis functions on plane triangles and tetrahedra. *Int. J. Numer. Meth. Eng.*, 58:1149–1165.
- Jaszczak, R. J. (1988). Tomographic radiopharmaceutical imaging. *Proc. IEEE*, 76:1079–1094.
- Johnson, C., MacLeod, R., and Ershler, P. (1992). A computer model for the study of electrical current flow in the human thorax. *Comp. in Bio. and Med.*, 22:305–323.
- Kaneko, Y., Yumoto, M., Shigeto, H., Ohtomo, S., Saito, O., and Takashima, Y. (2001). Effect of conductor model on source localization in case with source at the frontal base a realistic-shaped phantom study. In Nenonen, J., Ilmoniemi, R., and Katila, T., editors, *Proc. 12th Int. Conf. on Biomagnetism*, Espoo, Finland. Helsinki Univ. of Technology.
- Karjalainen, P., Kaipio, J., Koistinen, A., and Vauhkonen, M. (1999). Subspace regularization method for the single trial analysis of evoked potentials. *IEEE Trans. Biomed. Eng.*, 46:849–860.
- Karp, P. (1981). Cardiomagnetism. In Ern e, S., Hahlbohm, H., and L ubbig, H., editors, *Proc. Third Internat. Workshop On Biomagnetism*, pages 219–258. Walter de Gruyter, Berlin.
- Kass, M., Witkin, A., and Terzopoulos, D. (1987). Snakes: Active contour models. *Int. J. Comput. Vision*, 1:321–331.
- Kavanagh, R. N. and Darcey, T. (1978). Evaluation of methods for three dimensional localization of electrical sources in the human brain. *IEEE Trans. Biomed. Eng.*, 25:421–428.
- Knoll, G. F. (1983). Single-photon emission computed tomography. *Proc. IEEE*, 71:320–329.
- Koikkalainen, J. and L otj onen, J. (2004). Reconstruction of 3-d head geometry from digitized point sets: an evaluation study. *IEEE Trans. Inf. Tech. Biomed.*, 8:377–386.
- Leahy, R., Mosher, J., Spencer, M., Huang, M., and Lewine, J. (1998). A study of dipole localization accuracy for meg and eeg using a human skull phantom. *Electroenceph. Clin. Neurophysiol.*, 107:159–173.
- L otj onen, J., Reissman, P.-J., Magnin, I. E., and Katila, T. (1999). Model extraction from magnetic resonance volume data using the deformable pyramid. *Medical Image Analysis*, 3:387–406.
- L otj onen, J., Reissman, P.-J., Magnin, I. E., Nenonen, J., and Katila, T. (1998). A triangulation method of an arbitrary point set for biomagnetic problems. *IEEE Trans. Magnetism*, 34:2228–2233.
- Lynn, M. and Timlake, W. (1968). The use of multiple deflations in the numerical solution of singular systems of equations with applications to potential theory. *SIAM J. Numer. Anal.*, 5:303–322.

- MacLeod, R., Johnson, C., and Ershler, P. (1991). Construction of an inhomogeneous model of the human torso for use in computational electrocardiography. In *IEEE Eng. Med. Biol. Soc. Proceedings*, pages 688–689. IEEE Engineering in Medicine and Biology Society 13th Annual International Conference, IEEE Press.
- Malmivuo, J. and Plonsey, R. (1995). *Bioelectromagnetism - Principles and Applications of Bioelectric and Biomagnetic Fields*. Oxford University Press, New York.
- Malmivuo, J., Suihko, V., and Eskola, H. (1997). Sensitivity distributions of eeg and meg measurements. *IEEE Trans. Biomed. Eng.*, 44:196–208.
- Marin, G., Guerin, C., Baillet, S., Garnero, L., and Meunier, G. (1998). Influence of skull anisotropy for the forward and inverse problem in eeg: Simulation studies using fem on realistic head models. *Hum. Brain Mapp.*, 6:250–69.
- Meijs, J. and Peters, M. J. (1987). The EEG and MEG using a model of eccentric spheres to describe the head. *IEEE Trans. Biomed. Eng.*, 34:913–920.
- Meijs, J., Weier, O., and Peters, M. J. (1989). On the numerical accuracy of the boundary element method. *IEEE Trans. Biomed. Eng.*, 36:1038–1049.
- Mosher, J., Leahy, R., Huang, M., and Spencer, M. (1997). Modeling versus accuracy in eeg and meg data. In *Biomedizinische Technik*, volume 42, pages 5–8. NFSI.
- Mosher, J. C., Leahy, R. M., and Lewis, P. S. (1999). EEG and MEG: forward solutions for inverse problems. *IEEE Trans. Biomed. Eng.*, 46:245–259.
- Mosher, J. C., Lewis, P. S., and Leahy, R. M. (1992). Multiple dipole modeling and localization from spatio-temporal MEG data. *IEEE Trans. Biomed. Eng.*, 39:541–557.
- Nenonen, J., Purcell, C. J., Horacek, B. M., Stroink, G., and Katila, T. (1991). Magnetocardiographic functional localization using a current dipole in a realistic torso. *IEEE Trans. Biomed. Eng.*, 38:658–664.
- Nunez, P. L. (1981). *Electric fields of the brain: The Neurophysics of EEG*. Oxford University Press, New York.
- Nunez, P. L. (1990). Localization of brain activity with electroencephalography. *Adv. Neurol.*, 54:39–65.
- Okada, Y. (1981). Neurogenesis of evoked magnetic fields. In *Biomagnetism*, pages 399–408. Plenum, NY.
- Okada, Y. (1985). Discrimination of localized and distributed current dipole sources and localized single and multiple sources. In Weinberg, H., Stroink, G., and Katila, T., editors, *Biomagnetism*, pages 266–272. Pergamon, NY.
- Oostenveld, R. and Oostendorp, T. (2002). Validating the boundary element method for forward and inverse EEG computations in the presence of a hole in the skull. *Hum. Brain Mapp.*, 17:179–192.
- Pal, N. R. and Pal, S. K. (1993). A review on image segmentation techniques. *Pattern Recogn.*, 26:1277–1294.

- Plonsey, R. (1969). *Biomagnetic Phenomena*. McGraw-Hill, New York.
- Plonsey, R. (1981). Generation of magnetic fields by the human body(theory). In Ern , S., Hahlbohm, H., and L bbig, H., editors, *Proc. Third Internat. Workshop On Biomagnetism*, pages 177–200. Walter de Gruyter, Berlin.
- Poon, C., Braun, M., Fahrig, R., Ginige, A., and Dorrell, A. (1994). Segmentation of medical images using an active contour model incorporating region-based image features. In Robb, R. A., editor, *Visualization in Biomedical Computing*, number 2359 in SPIE, pages 90–97, Rochester, USA.
- Pullan, A. (1996). A high-order coupled finite element/boundary element torso model. *IEEE Trans. Biomed. Eng.*, 43:292–298.
- Ramon, C., Czapski, P., Haueisen, J., Huntsman, L., Nowak, H., Bardy, G. H., Leder, U., Kim, Y., and Nelson, J. (1998). MEG simulations with a realistic heart-torso model. *IEEE Trans. Biomed. Eng.*, 45:1323–1331.
- Rockel, A., Hiorns, R., and Powell, T. (1980). The basic uniformity in structure of the neurocortex. *Brain*, 103:221–244.
- Rush, S. and Driscoll, D. A. (1968). Current distribution in the brain from surface electrodes. *Anesth. Analg.*, 47:717–723.
- Rush, S. and Driscoll, D. A. (1969). EEG electrode sensitivity: An application of reciprocity. *IEEE Trans. Biomed. Eng.*, 16:15–22.
- Salu, Y., Cohen, L. G., Rose, D., Sato, S., Kufta, C., and Hallett, M. (1990). An improved method for localizing electric brain dipoles. *IEEE Trans. Biomed. Eng.*, 37:699–705.
- Sandor, S. and Leahy, R. M. (1997). Surface-based labeling of cortical anatomy using a deformable atlas. *IEEE Trans. Med. Imag.*, 16:41–54.
- Sarvas, J. (1987). Basic mathematical and electromagnetic concepts of the biomagnetic inverse problem. *Phys. Med. Biol.*, 32:11–22.
- Schlitt, H. A., Heller, L., Aaron, R., Best, E., and Ranken, D. (1995). Evaluation of boundary element methods for the eeg forward problem: Effect of linear interpolation. *IEEE Trans. Biomed. Eng.*, 42:52–58.
- Seo, J., Pyo, H., Park, C., Kwon, O., and Woo, E. (2004). Image reconstruction of anisotropic conductivity tensor distribution in MREIT: computer simulation study. *Phys. Med. Biol.*, 49:4371–4382.
- Snell, J. W. (1995). Model-based boundary estimation of complex objects using hierarchical active surface templates. *Pattern Recogn.*, 28:1599–1609.
- Srebro, R., Oguz, R. M., Hughlett, K., and Purdy, P. D. (1993). MEG versus EEG localization test using implanted sources in the human brain. *IEEE Trans. Biomed. Eng.*, 40:509–516.
- Stok, C. J. (1986). *The Inverse Problem in EEG and MEG with Application to Visual Evoked Responses*. PhD thesis, University of Twente, Twente, The Netherlands.

- Sun, M. (1997). An efficient algorithm for computing multishell spherical volume conductor models in EEG dipole source localization. *IEEE Trans. Biomed. Eng.*, 44:1243-1252.
- Tanzer, I. O. and Gençer, N. G. (1997). A new boundary element method formulation of the forward problem solution of electro-magnetic source imaging. In *Proc. 19th Ann. Int. Conf. IEEE Eng. Med. Biol. Soc.*, pages 2100–2103, Chicago, IL, USA. IEEE.
- Taulu, S., Simola, J., and Kajola, M. (2005). Applications of the signal space separation method. *IEEE Trans. Signal Processing*, 53:3359–3372.
- Tek, H. and Kimia, B. (1995). Volumetric segmentation of medical images by three-dimensional bubbles. *Comput. Vis. Image. Und.*, 65:1599–1609.
- Tenner, U., Wiechmann, H., Brauer, H., Gomonov, D., Arlt, A., and Ziolkowski, M. (1997). Realistic thorax modeling for biomagnetic and bioelectric source reconstruction techniques. In *Biomedizinische Technik*, volume 42, pages 96–98. NFSI-Noninvasive Functional Source Imaging.
- Thevenet, M., Bertrand, O., Perrin, F., Dumont, T., and Pernier, J. (1991). The finite element method for a realistic head model of electrical brain activities: Preliminary results. *Clin. Phys. Physiol. M.*, 12:89–94.
- Thompson, P. and Toga, A. (1996). A surface-based technique for warping three-dimensional images of the brain. *IEEE Trans. Med. Imag.*, 15:402–417.
- Tissari, S. and Rahola, J. (2003). Error analysis of a Galerkin method to solve the forward problem in MEG using the boundary element method. *Comput. Meth. Prog. Bio.*, 72:209–222.
- Tonon, F., Pan, E., and Amadei, B. (2000). Greens functions and bem formulation for 3d anisotropic media. *Computers and Structures*, 79:469–482.
- Tuch, D., Wedeen, V., Dale, A., George, J., and Belliveau, J. (2001). Conductivity tensor mapping of the human brain using diffusion tensor MRI. *PNAS*, 20:11697–11701.
- Uitert, R., Weinstein, D., and Johnson, C. (2002). Can a spherical model substitute for a realistic head model in forward and inverse meg simulations? In *Proc. 13th Int. Conf. on Biomagnetism*, pages 798–800, Jena, Germany.
- Uitert, R., Weinstein, D., and Johnson, C. (2003). Volume currents in forward and inverse magnetoencephalographic simulations using realistic head models. *Ann. Biomed. Eng.*, 31:21–31.
- Uutela, K., M, M. H., and Somersalo, E. (1999). Visualization of magnetoencephalographic data using minimum current estimates. *Neuroimage*, 10:173–180.
- van den Broek, B. (1997). *Volume conduction effects in EEG and MEG*. PhD thesis, University of Twente, Enschede, Netherlands.

- van den Broek, S., Zhou, H., and Peters, M. (1996). Computation of neuromagnetic fields using finite-element method and Biot-Savart law. *Med. Biol. Eng. Comput.*, 34:21–26.
- van Oosterom, A. and Huiskamp, G. J. (1991). A realistic torso model for magneto-cardiography. *Int. J. Card. Imaging.*, 7:169–176.
- Vanrumste, B. (2001). *EEG dipole source analysis in a realistic head model*. PhD thesis, University of Gent, Belgium.
- Vigario, R. and Oja, E. (2000). Independence: A new criterion for the analysis of the electromagnetic fields in the global brain. *Neural Networks*, 13:891–907.
- Vrba, J. and E. Robinson, S. (2001). Signal processing in magnetoencephalography. *Methods*, 25:249–271.
- Wagner, M. and Fuchs, M. (2001). Integration of functional mri, structural mri, eeg, and meg. *IJBEM, Int. J. Bioelectromag*, 3.
- Wang, Y., Adali, T., Kung, S., and Szabo, Z. (1998). Quantification and segmentation of brain tissue from mr images: A probabilistic neural network approach. *IEEE Trans. Image Processing*, 7:1165–1181.
- Wells, W. M., Grimson, W. L., Kikinis, R., and Jolesz, F. A. (1995). Adaptive segmentation of MRI data. In Ayache, N., editor, *Computer Vision, Virtual Reality and Robotics in Medicine*. Springer-Verlag.
- Wieringa, H. J. (1993). *MEG, EEG and the Integration with Magnetic Resonance Images*. PhD thesis, University of Twente, Enschede, The Netherlands.
- Wikswow, J., Barach, P., and Freeman, J. (1980). Magnetic field of a nerve impulse: first measurements. *Science*, 208:53–55.
- Wikswow, J. P. (1983). Cellular action currents. In Williamson, S. J., Romani, G. L., Kaufman, L., and Modena, I., editors, *Biomagnetism, An Interdisciplinary Approach*, pages 173–207. Plenum, NY.
- Williamson, S. (1990). *Theory of neuroelectric and neuromagnetic fields*. Advances in audiology. Auditory Evoked Magnetic Fields and Electric Potentials.
- Williamson, S. and Kaufman, L. (1983). *Neuromagnetism*. NATO Advanced Study Institute Series. Plenum Press, New York.
- Wilson, F. N. and Bayley, R. H. (1950). The electric field of an eccentric dipole in a homogeneous spherical conducting medium. *Circulation*, 1:84–92.
- Wolters, C. (2003). *Influence of Tissue Conductivity Inhomogeneity and Anisotropy on EEG and MEG based Source Localization in the Human Brain*. PhD thesis, MPI of Cognitive Neuroscience Leipzig, Leipzig Univ., ISBN: 3-936816-11-5. MPI Series in Cognitive Neuroscience.

- Wolters, C., Anwander, A., Tricoche, X., Weinstein, D., Koch, M., and MacLeod, R. (2005). Influence of tissue conductivity anisotropy on eeg/meg field and return current computation in a realistic head model: A simulation and visualization study using high-resolution finite element modeling. *Neuroimage*, doi:10.1016/j.neuroimage.2005.10.014.
- Wolters, C. H., Kuhn, M., Anwander, A., and Reitzinger, S. (2002). A parallel algebraic multigrid solver for finite element method based source localization in the human brain. *Comp. Vis. Sci.*, 5:165–177.
- Yan, M. and Karp, J. (1995). *An Adaptive Bayesian Approach to Three dimensional MR Brain Segmentation*, pages 140–145. Kluwer, Dordrecht, Germany.
- Yan, Y., Nunez, P. L., and Hart, R. T. (1991). A finite element model for the human head: Scalp potentials due to dipole sources. *Med. Biol. Eng. Comput.*, 29:475–481.
- Yao, D. (2000). Electric potential produced by a dipole in a homogeneous conducting sphere. *IEEE Trans. Biomed. Eng.*, 47:964–6.
- Yezzi, A., Kichenassamy, S., Kumar, A., Olver, P., and Tannenbaum, A. (1997). A geometric snake model for segmentation of medical imagery. *IEEE Trans. Med. Imag.*, 16:199–209.
- Zanow, F. (1997). *Realistically shaped models of the head and their application to EEG and MEG*. PhD thesis, University of Twente, The Netherlands.
- Zanow, F. and Peters, M. J. (1995). Individually shaped volume conductor models of the head in EEG source localisation. *Med. Biol. Eng. Comput.*, 33:582–588.
- Zhang, Z. (1995). A fast method to compute surface potentials generated by dipoles within multilayer anisotropic spheres. *Phys. Med. Biol.*, 40:335–49.
- Zhou, H. and van Oosterom, A. (1992). Computation of the potential distribution in a four layer anisotropic concentric spherical volume conductor. *IEEE Trans. Biomed. Eng.*, 39:154–158.
- Zhou, H. and van Oosterom, A. (1994). Application of the boundary element method to the solution of anisotropic electromagnetic problems. *Med. Biol. Eng. and Comput.*, 32:399–405.
- Zimmerman, J. E., Thiene, P., and Hardings, J. (1970). Design and operation of stable r-f biased superconducting point-contact quantum devices. *J. Appl. Phys.*, 41:1572–1580.



ISBN 951-22-8090-6
ISBN 951-22-8091-4 (PDF)
ISSN 1795-2239
ISSN 1795-4584 (PDF)